SÜLEYMAN DEMİREL UNIVERSITY

JOURNAL OF CERAMICS AND COMPOSITES

VOLUME:01 ISSUE:02 YEAR:2025 e-ISSN: 3062-293X

SÜLEYMAN DEMİREL UNIVERSITY

SÜLEYMAN DEMİREL UNIVERSITY

CONTENTS

Research Article

JOURNAL OF CERAMICS AND COMPOSITES

e-ISSN: 3062-293X

Buckling analysis of porous power-law and sigmoid functionally graded sandwich plates

Lazreg Hadji[a,*], Nafissa Zouatnia[b], Burak İkinci[c]

[a]Department of Civil Engineering, University of Tiaret, Tiaret 14000, Algeria
[b]Department of Civil Engineering, University of Tiaret, Tiaret 14000, Algeria
[c]Department of Civil Engineering, Faculty of Engineering and Natural Sciences, Süleyman Demirel University, Isparta, Türkiye

Highlights

- Buckling of porous functionally graded sandwich plates according to power-law and sigmoid law
- Refined shear deformation plate theory
- Analysis carried out using analytical method
- Different porosity models

Abstract

In this study, an advanced shear deformation plate theory is proposed to analyze the buckling behaviour of functionally graded sandwich plates. A novel definition of porosity distribution which accounts for both material composition and sandwich plate architecture, is included. The material properties of the functionally graded material layers are assumed to vary continuously through the plate thickness, described by either a power-law or sigmoid function based on the volume fractions of materials. The core is a homogeneous ceramic layer, while the outer layers on both sides are considered functionally graded across thickness. The virtual displacement principle is used to formulate the governing equations. The Navier method is utilized to derive a closed-form solution for a simply supported rectangular plate. Numerical results are provided to demonstrate the influence of material distribution, sandwich plate geometry, and porosity on the buckling loads of FG sandwich plates. The proposed theory is compared with results from previous studies to validate the accuracy and reliability. The proposed theory is accurate and simple in solving the buckling behavior of porous power-law and sigmoid functionally graded sandwich plates FGM plates.

Information

Received:
27.02.2025
Received in revised:
06.04.2025
Accepted:
14.04.20205

Keywords: *Buckling, functionally graded materials, refined plate theory, porosity*

1. Introduction

Sandwich structures are developed and utilized over the past fifty years due to their superior mechanical properties such higher bending rigidity, low specific weight, vibration, isolation, and anti-fatigue characteristics. These properties enable effective usage of sandwich structures for large-scale civil infrastructure projects such as bridges and industrial buildings.

Typical sandwich structures are made of two thin face sheets and a core. Face sheets have high rigidity, such are metal or laminated composite materials, whereas relative thick, lightweight core, often consists of low-strength material such as polymeric foam. Adhesive bonding is used to join the components, ensuring efficient load transfer within the structure.

Functionally graded materials (FGMs), a type of advanced [1,2] inhomogeneous composites, were initially proposed for eliminating thermal stress [3], have gained increasing attention for their utility in high-temperature engineering environments. To investigate the thermo-mechanical behavior of FGMs, many studies have been conducted focusing on understanding the mechanics and response of FGM structures [4,5].

FGMs have been the subject of extensive research on structural behavior and mechanics because of their wide applications. The versatility of functionally graded (FG) plates and shells made them particular interest. Shear deformation plate theory, the finite-element method, and energy methods, have been employed to examine FG structures. Notably, Cheng and Batra [6] examined the buckling and steady-state vibrations of simply supported FG polygonal plates based on Reddy's plate theory. Meanwhile, Reddy [7] provided solutions for the static

*Corresponding author: lazreg.hadji@univ-tiaret.dz (Lazreg, Hadji), +213-551954112

behavior of FG rectangular plates using his third-order shear deformation plate theory. Praveen and Reddy [8] further explored the nonlinear static and dynamic responses of FG ceramic-metal plates using a plate finite element that includes transverse shear strains, rotating inertia, and relatively large rotations in the von Karman sense.

FG sandwiches show promise in mitigating large interfacial shear stress concentrations due to the gradual variation of material properties at the face sheet-core interface. Pan and Han [9] analyzed the static response of multilayered rectangular plates made of FG anisotropic and linear magneto-electro-elastic materials.

Micro-voids or porosities can occur due to the significant differences in solidification temperatures between the constituent materials during the process of FGM manufacturing [10]. Wattanasakulpong et al. [11] examined the porous FGM samples produced through a multistep sequential infiltration technique, and Wattanasakulpong and Ungbhakorn [12] examined linear and nonlinear vibration problems of elastically end-restrained porous FG beams. Ould Larbi et al. [13] studied in-plane bi-directional porous FG plates under various boundary conditions for buckling problems, employing a simple refined plate theory. Draouche et al. [14] studied the impact of porosity and boundary conditions on the dynamic properties of cracked FG plates. Ait Atmane et al. [15] investigated effect of thickness stretching and porosity on mechanical response of functionally graded beams resting on elastic foundations. Recently Meski et al. [16] used a simple refined plate theory for buckling problems of in-plane bi-directional functionally graded plates with porosity under various boundary conditions. Nebab et al. [17] studied fundamental frequencies of cracked FGM beams with influence of porosity and Winkler/Pasternak/Kerr foundation support using a new quasi-3D HSDT.

To our knowledge, there has been no investigation on buckling power-law and sigmoid functionally graded sandwich plates with porosity that uses the four-variable refined plate theory (RPT). This study aims to conduct a buckling analysis of power-law and sigmoid functionally graded sandwich plates with porosity utilizing the RPT. Power-law and sigmoid functions are widely used to model material property variations due to mathematical simplicity and practical advantage characterictics. The power-law function is computationally efficient, while the sigmoid function offers a smooth transition, ideal for modeling gradual changes in material behavior, such as the transition from elastic to plastic deformation. Unlike any other theories, presented theory gives rise to only four governing equations. The number of unknown functions involved is only four, as against five in case of simple shear deformation theories of Mindlin and Reissner (first shear deformation theory). The material property variation and porosity distribution are critical to the buckling behavior of functionally graded sandwich plates due to their direct impact on the mechanical response and stability of the structure under load. To investigate the effect of porosity, different porosity models were used, where porosities are assumed to be distributed along FG sandwich layers. The results are compared with previous findings to represent the influence of this approach, as well as the presentation of new results that may serve as a basis for future works.

2. Problem formulation

A rectangular plate with the length a, width b, and a uniform thickness h is shown in Figure 1.

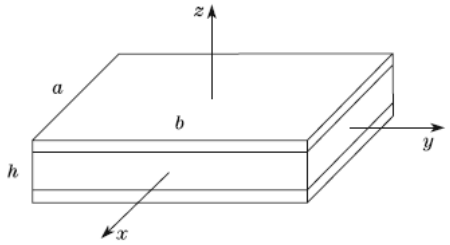

Figure 1. Geometry of the rectangular FG sandwich plate with uniform thickness in rectangular Cartesian coordinates

The plate is composed of a ceramic and metallic mixture, with mechanical properties varying continuously in both directions: x- and y-axes. The Cartesian coordinate system is also shown in the Figure 1.

2.1. Power-law FG sandwich plate

Based on a power-law function (P-FG), the present plate is composed of three layers: two FG layers and an isotropic core. While the face layers are graded from metal to ceramic, the core layer is made of ceramic. The volume fraction $V^{(n)}$ of layer $(n=1,2,3)$ can be expressed as

$$V^{(1)}(z)=\left(\frac{z-h_1}{h_2-h_1}\right)^n \tag{1a}$$

$$V^{(2)}(z)=1 \tag{1b}$$

$$V^{(3)}(z)=\left(\frac{z-h_4}{h_3-h_4}\right)^n \tag{1c}$$

2.2. Sigmoid FG sandwich plate

According to a sigmoid function, the volume fraction varies through-the-thickness [18]:

$$V_1^{(1)}(z)=\frac{1}{2}\left(\frac{z-h_1}{h_m-h_1}\right)^n,\ h_1\le z\le h_m \tag{2a}$$

$$V_2^{(1)}(z)=1-\frac{1}{2}\left(\frac{z-h_2}{h_m-h_2}\right)^n,\ h_m\le z\le h_2 \quad (2b)$$

$$V^{(2)}(z)=1,\ h_2\le z\le h_3 \quad (2c)$$

$$V_1^{(3)}(z)=1-\frac{1}{2}\left(\frac{z-h_3}{h_n-h_3}\right)^n,\ h_3\le z\le h_n \quad (2d)$$

$$V_2^{(3)}(z)=\frac{1}{2}\left(\frac{z-h_4}{h_n-h_4}\right)^n,\ h_n\le z\le h_4 \quad (2e)$$

Where

$$h_m=(h_1+h_2)/2 \text{ and } h_n=(h_3+h_4)/2 \quad (2f)$$

denotes the middle surface positions of the bottom and the top layer, respectively.

3. Porosity-dependent FG sandwich plates

Numerous porosity distribution models have been proposed by researchers to evaluate the effective material properties of porous FG plate [12]. In this study, four different porosity types are used, with the porosities distributed independently within each FGM layer of the sandwich.

3.1. Imperfect I: Even porosities (IP-I)

The FG sandwich plate is made of a blend of metal and ceramic and the influence of porosity is included. The FG sandwich layers have porosity which is evenly distributed, and the core layer is nonporous ceramic. The effective material properties $\Gamma^{(n)}$ of layer n $(n=1,2,3)$ with evenly distributed porosities (imperfect I) are expressed using the rule of mixture and can be stated as [18]

$$\begin{aligned}\Gamma^{(1)}(z)&=(\Gamma_c-\Gamma_m)V^{(1)}(z)+\Gamma_m-\frac{\xi}{2}(\Gamma_c+\Gamma_m)\\ \Gamma^{(2)}(z)&=(\Gamma_c-\Gamma_m)V^{(2)}(z)+\Gamma_m\\ \Gamma^{(3)}(z)&=(\Gamma_c-\Gamma_m)V^{(3)}(z)+\Gamma_m-\frac{\xi}{2}(\Gamma_c+\Gamma_m)\end{aligned} \quad (3)$$

where ξ denotes the porosity coefficient $(\xi \prec\prec 1)$. Γ_c and Γ_m are the corresponding properties of the ceramic and metal, respectively.

3.2 Imperfect II: Uneven porosities (IP-II)

The porosities distributed functionally across the thickness direction of the FG sandwich as follows:

$$\begin{aligned}\Gamma^{(1)}(z)&=(\Gamma_c-\Gamma_m)V^{(1)}(z)+\Gamma_m-\frac{\xi}{2}(\Gamma_c+\Gamma_m)\left[1-\frac{|2z-h_1-h_2|}{h_2-h_1}\right]\\ \Gamma^{(2)}(z)&=(\Gamma_c-\Gamma_m)V^{(2)}(z)+\Gamma_m\\ \Gamma^{(3)}(z)&=(\Gamma_c-\Gamma_m)V^{(3)}(z)+\Gamma_m-\frac{\xi}{2}(\Gamma_c+\Gamma_m)\left[1-\frac{|2z-h_4-h_3|}{h_4-h_3}\right]\end{aligned} \quad (4)$$

3.3 Imperfect III: Logarithmic-uneven porosities (IP-III)

Based on a logarithmic function, IP-III model can be formulated as

$$\begin{aligned}\Gamma^{(1)}(z)&=(\Gamma_c-\Gamma_m)V^{(1)}(z)+\Gamma_m-\log\left(1+\frac{\xi}{2}\right)(\Gamma_c+\Gamma_m)\left[1-\frac{|2z-h_1-h_2|}{h_2-h_1}\right]\\ \Gamma^{(2)}(z)&=(\Gamma_c-\Gamma_m)V^{(2)}(z)+\Gamma_m\\ \Gamma^{(3)}(z)&=(\Gamma_c-\Gamma_m)V^{(3)}(z)+\Gamma_m-\log\left(1+\frac{\xi}{2}\right)(\Gamma_c+\Gamma_m)\left[1-\frac{|2z-h_4-h_3|}{h_4-h_3}\right]\end{aligned} \quad (5)$$

3.4 Imperfect IV: Linear-uneven porosities (IP-VI)

At the outer surfaces of the sandwich, the density of porosity is low and at the two interfaces positions, the density of porosity is higher and changes across the FG layers with linear function as

$$\begin{aligned}\Gamma^{(1)}(z)&=(\Gamma_c-\Gamma_m)V^{(1)}(z)+\Gamma_m-\frac{\xi}{2}(\Gamma_c+\Gamma_m)\left[1-\frac{z-h_2}{h_1-h_2}\right]\\ P^{(2)}(z)&=(\Gamma_c-\Gamma_m)V^{(2)}(z)+\Gamma_m\\ P^{(3)}(z)&=(\Gamma_c-\Gamma_m)V^{(3)}(z)+\Gamma_m-\frac{\xi}{2}(\Gamma_c+\Gamma_m)\left[\frac{z-h_4}{h_3-h_4}\right]\end{aligned} \quad (6)$$

4. Mathematical Formulation

4.1. Kinematic, strain and stress relations

The assumed field of displacements can be defined by the subsequent equations [19]:

$$\begin{aligned}u(x,y,z)&=u_0(x,y)-z\frac{\partial w_b}{\partial x}-f(z)\frac{\partial w_s}{\partial x}\\ v(x,y,z)&=v_0(x,y)-z\frac{\partial w_b}{\partial y}-f(z)\frac{\partial w_s}{\partial y}\\ w(x,y,z)&=w_b(x,y)+w_s(x,y)\end{aligned} \quad (7)$$

In which u_0 and v_0 denote the displacement functions of the middle surfaces of the FG plate. Also, *f(z)* refers to the variation of the transverse shear strain along with the plate thickness. In this study

$$f(z)=z\left[1+\frac{3\pi}{2}\sec h\left(\frac{1}{2}\right)^2\right]-\frac{3\pi}{2}h\tanh\left(\frac{z}{h}\right) \quad (8)$$

The nonzero strains relating to the displacement field are:

$$\begin{Bmatrix}\varepsilon_x\\ \varepsilon_y\\ \gamma_{xy}\end{Bmatrix}=\begin{Bmatrix}\varepsilon_x^0\\ \varepsilon_y^0\\ \gamma_{xy}^0\end{Bmatrix}+z\begin{Bmatrix}k_x^b\\ k_y^b\\ k_{xy}^b\end{Bmatrix}+f(z)\begin{Bmatrix}k_x^s\\ k_y^s\\ k_{xy}^s\end{Bmatrix} \quad (9)$$

$$\begin{Bmatrix}\gamma_{yz}\\ \gamma_{xz}\end{Bmatrix}=g(z)\begin{Bmatrix}\gamma_{yz}^s\\ \gamma_{xz}^s\end{Bmatrix}$$

Where

$$\begin{Bmatrix}\varepsilon_x^0\\ \varepsilon_y^0\\ \gamma_{xy}^0\end{Bmatrix}=\begin{Bmatrix}\dfrac{\partial u_0}{\partial x}\\ \dfrac{\partial v_0}{\partial x}\\ \dfrac{\partial u_0}{\partial y}+\dfrac{\partial v_0}{\partial x}\end{Bmatrix},\begin{Bmatrix}k_x^b\\ k_y^b\\ k_{xy}^b\end{Bmatrix}=\begin{Bmatrix}-\dfrac{\partial^2 w_b}{\partial x^2}\\ -\dfrac{\partial^2 w_b}{\partial y^2}\\ -2\dfrac{\partial^2 w_b}{\partial x\partial y}\end{Bmatrix} \quad (10a)$$

$$\begin{Bmatrix}k_x^s\\ k_y^s\\ k_{xy}^s\end{Bmatrix}=\begin{Bmatrix}-\dfrac{\partial^2 w_s}{\partial x^2}\\ -\dfrac{\partial^2 w_s}{\partial y^2}\\ -2\dfrac{\partial^2 w_s}{\partial x\partial y}\end{Bmatrix},\begin{Bmatrix}\gamma_{yz}^s\\ \gamma_{xz}^s\end{Bmatrix}=g(z)\begin{Bmatrix}\dfrac{\partial w_s}{\partial y}\\ \dfrac{\partial w_s}{\partial x}\end{Bmatrix} \quad (10b)$$

Then

$$g(z)=1-\frac{df(z)}{dz} \quad (10c)$$

For elastic and isotropic FGMs, the constitutive relations can be written as:

$$\begin{Bmatrix}\sigma_x\\ \sigma_y\\ \tau_{yz}\\ \tau_{xz}\\ \tau_{xy}\end{Bmatrix}^{(n)}=\begin{bmatrix}C_{11}&C_{12}&0&0&0\\ C_{12}&C_{22}&0&0&0\\ 0&0&C_{44}&0&0\\ 0&0&0&C_{55}&0\\ 0&0&0&0&C_{66}\end{bmatrix}^{(n)}\begin{Bmatrix}\varepsilon_x\\ \varepsilon_y\\ \gamma_{yz}\\ \gamma_{xz}\\ \gamma_{xy}\end{Bmatrix} \quad (11)$$

where

$$C_{11}(z)=\frac{E(z)}{\left(1-\nu^2\right)},\ C_{12}(z)=\nu C_{11}(z) \quad (12a)$$

and

$$C_{44}(z)=C_{55}(z)=C_{66}(z)=\frac{E(z)}{2(1+\nu)} \quad (12b)$$

5. Governing equations

"By employing the principle of virtual displacements, the governing equilibrium equations can be obtained. In the present case, the virtual work principle provides

$$\int_{-h/2}^{h/2}\int_{\Omega}\begin{bmatrix}\sigma_x\delta\varepsilon_x+\sigma_y\delta\varepsilon_y+\tau_{xy}\delta\gamma_{xy}\\ +\tau_{xz}\delta\gamma_{xz}+\tau_{yz}\delta\gamma_{yz}\end{bmatrix}d\Omega dz.-\int_{\Omega}\overline{N}\delta w d\Omega=0 \quad (13)$$

with

$$\overline{N}=N_x^0\frac{\partial^2(w_b+w_s)}{\partial x^2}+N_y^0\frac{\partial^2(w_b+w_s)}{\partial y^2}+N_{xy}^0\frac{\partial^2(w_b+w_s)}{\partial x\partial y} \quad (14)$$

From Eq. (13), the equilibrium equations can be formulated by integrating the displacement gradients by parts and setting the coefficients δu_0, δv_0, δw_b, and δw_s independently to zero. Therefore, the equilibrium equations associated with the present refined shear deformation plate theory:

$$\begin{aligned}
&\delta u_0:\ \frac{\partial N_x}{\partial x}+\frac{\partial N_{xy}}{\partial y}=0\\
&\delta v_0:\ \frac{\partial N_{xy}}{\partial x}+\frac{\partial N_y}{\partial y}=0\\
&\delta w_b:\ \frac{\partial^2 M_x^b}{\partial x^2}+2\frac{\partial^2 M_{xy}^b}{\partial x\partial y}+\frac{\partial^2 M_y^b}{\partial y^2}+\overline{N}=0\\
&\delta w_s:\ \frac{\partial^2 M_x^s}{\partial x^2}+2\frac{\partial^2 M_{xy}^s}{\partial x\partial y}+\frac{\partial^2 M_y^s}{\partial y^2}+\frac{\partial S_{xz}^s}{\partial x}+\frac{\partial S_{yz}^s}{\partial y}+\overline{N}=0
\end{aligned} \quad (15)$$

The equations of equilibrium can be formulated in terms of displacements. (u_0, v_0, w_b, w_s) and the appropriate equations take the form:

$$\begin{aligned}
&(A_{12}+A_{66})\frac{\partial^2 u_0}{\partial x\partial y}+A_{66}\frac{\partial^2 v_0}{\partial x^2}+A_{22}\frac{\partial^2 v_0}{\partial y^2}-(B_{12}+2B_{66})\frac{\partial^3 w_b}{\partial x^2\partial y}\\
&-B_{22}\frac{\partial^3 w_b}{\partial y^3}-B_{22}^s\frac{\partial^3 w_s}{\partial y^3}-\left(B_{12}^s+2B_{66}^s\right)\frac{\partial^3 w_s}{\partial x^2\partial y}=0
\end{aligned} \quad (16a)$$

$$\begin{aligned}
&(A_{12}+A_{66})\frac{\partial^2 u_0}{\partial x\partial y}+A_{66}\frac{\partial^2 v_0}{\partial x^2}+A_{22}\frac{\partial^2 v_0}{\partial y^2}-(B_{12}+2B_{66})\frac{\partial^3 w_b}{\partial x^2\partial y}\\
&-B_{22}\frac{\partial^3 w_b}{\partial y^3}-B_{22}^s\frac{\partial^3 w_s}{\partial y^3}-\left(B_{12}^s+2B_{66}^s\right)\frac{\partial^3 w_s}{\partial x^2\partial y}=0
\end{aligned} \quad (16b)$$

$$B_{11}\frac{\partial^3 u_0}{\partial x^3}+\left(B_{12}+2B_{66}\right)\frac{\partial^3 u_0}{\partial x\partial y^2}+\left(B_{12}+2B_{66}\right)\frac{\partial^3 v_0}{\partial x^2\partial y}+B_{22}\frac{\partial^3 v_0}{\partial y^3}$$
$$-D_{11}\frac{\partial^4 w_b}{\partial x^4}-2\left(D_{12}+2D_{66}\right)\frac{\partial^4 w_b}{\partial x^2\partial y^2}-D_{22}\frac{\partial^4 w_b}{\partial y^4}-D_{11}^s\frac{\partial^4 w_s}{\partial x^4} \quad (16c)$$
$$-2\left(D_{12}^s+2D_{66}^s\right)\frac{\partial^4 w_s}{\partial x^2\partial y^2}-D_{22}^s\frac{\partial^4 w_s}{\partial y^4}+\overline{N}=0$$

$$B_{11}^s\frac{\partial^3 u_0}{\partial x^3}+\left(B_{12}^s+2B_{66}^s\right)\frac{\partial^3 u_0}{\partial x\partial y^2}+\left(B_{12}^s+2B_{66}^s\right)\frac{\partial^3 v_0}{\partial x^2\partial y}+B_{22}^s\frac{\partial^3 v_0}{\partial y^3}$$
$$-D_{11}^s\frac{\partial^4 w_b}{\partial x^4}-2\left(D_{12}^s+2D_{66}^s\right)\frac{\partial^4 w_b}{\partial x^2\partial y^2}-D_{22}^s\frac{\partial^4 w_b}{\partial y^4}-H_{11}^s\frac{\partial^4 w_s}{\partial x^4} \quad (16d)$$
$$-2\left(H_{12}^s+2H_{66}^s\right)\frac{\partial^4 w_s}{\partial x^2\partial y^2}-H_{22}^s\frac{\partial^4 w_s}{\partial y^4}+A_{55}^s\frac{\partial^2 w_s}{\partial x^2}+A_{44}^s\frac{\partial^2 w_s}{\partial y^2}+\overline{N}=0$$

6. The Solution of the Problem

In this section, an exact solution for the buckling analysis of FG sandwich plates i.e. Eqs. (16) is presented. The boundary conditions for an arbitrary edge with simply supported condition are:

$$v_0=w_b=\partial w_b/\partial y=w_s=\partial w_s/\partial y=0 \quad (17a)$$

at $x=0,a$

$$u_0=w_b=\partial w_b/\partial x=w_s=\partial w_s/\partial x=0 \quad (17b)$$

at $y=0,b$

The displacement functions that satisfy the equations of boundary conditions (17) are selected as the following Fourier series:

$$\begin{Bmatrix}u_0\\v_0\\w_b\\w_s\end{Bmatrix}=\sum_{m=1}^{\infty}\sum_{n=1}^{\infty}\begin{Bmatrix}U_{mn}\cos(\lambda x)\sin(\mu y)\\V_{mn}\sin(\lambda x)\cos(\mu y)\\W_{bmn}\sin(\lambda x)\sin(\mu y)\\W_{smn}\sin(\lambda x)\sin(\mu y)\end{Bmatrix} \quad (18)$$

Where U_{mn}, V_{mn}, W_{bmn}, and W_{smn} are arbitrary parameters and $\lambda=m\pi/a$ and $\mu=n\pi/b$.

By substituting Eqs. (18) into Eqs. (16), the analytical solutions can be derived as:

$$\begin{bmatrix}S_{11}&S_{12}&S_{13}&S_{14}\\S_{12}&S_{22}&S_{23}&S_{24}\\S_{13}&S_{23}&S_{33}+k&S_{34}+k\\S_{14}&S_{24}&S_{34}+k&S_{44}+k\end{bmatrix}\begin{Bmatrix}U_{mn}\\V_{mn}\\W_{bmn}\\W_{smn}\end{Bmatrix}=\begin{Bmatrix}0\\0\\0\\0\end{Bmatrix} \quad (19)$$

In which

$$S_{11}=A_{11}\lambda^2+A_{66}\mu^2$$
$$S_{12}=\lambda\mu\left(A_{12}+A_{66}\right)$$
$$S_{13}=-\lambda\left(B_{11}\lambda^2+\left(B_{12}+2B_{66}\right)\mu^2\right)$$
$$S_{14}=-\lambda\left(B_{11}^s\lambda^2+\left(B_{12}^s+2B_{66}^s\right)\mu^2\right)$$
$$S_{22}=A_{66}\lambda^2+A_{22}\mu^2$$
$$S_{23}=-\mu\left(\left(B_{12}+2B_{66}\right)\lambda^2+B_{22}\mu^2\right) \quad (20)$$
$$S_{24}=-\mu\left(\left(B_{12}^s+2B_{66}^s\right)\lambda^2+B_{22}^s\mu^2\right)$$
$$S_{33}=D_{11}\lambda^4+2(D_{12}+2D_{66})\lambda^2\mu^2+D_{22}\mu^4$$
$$S_{34}=D_{11}^s\lambda^4+2\left(D_{12}^s+2D_{66}^s\right)\lambda^2\mu^2+D_{22}^s\mu^4$$
$$S_{44}=H_{11}^s\lambda^4+2\left(H_{12}^s+2H_{66}^s\right)\lambda^2\mu^2+H_{22}^s\mu^4$$
$$+A_{55}^s\lambda^2+A_{44}^s\mu^2$$
$$k=-N_0\left(\lambda^2+\gamma\mu^2\right)$$

7. Numerical results and discussion

In this study, various examples are presented to illustrate the effect of porosity on the buckling of FG sandwich plates using the present RPT. The FG plate is made of aluminum (Al) and alumina (Al_2O_3) and the material properties:

Ceramic (Alumina, Al2O3): $E_c=380GPa$, $\nu=0.3$

Metal (Aluminum, Al): $E_m=70GPa$, $\nu=0.3$

For convenience, the following dimensionless variable is applied to illustrate some numerical results graphically and reported the other in tabular form. Non-dimensional critical buckling load (NDCBL):

$$\overline{N}=\frac{N_{cr}a^2}{100h^3E_0}$$

In which the reference values of Young's modulus and material density are taken as $E_0=1$ GPa.

Table 1 shows the influence of volume fraction index, n, the side-to thickness ratio, *a/h,* and the scheme of the sandwich on the NDCBL of two models of FG sandwich plates using CPT, FPT, TSDT, SSDT [20], simple higher-order shear deformation theory of Daikh [21], and the present RPT. It can be concluded that the NDCBLs decrease with increase of n. Results computed by the proposed RPT are in good agreement with the results of other HSDTs. Furthermore, it can be concluded that the

difference between the shear deformation theories and the CPT decreases as the n increases.

In Table 2, the effect of the four models of porosities distribution on the NDCBL of square P-FG and S-FG sandwich plates is illustrated using the present refined shear deformation theory. The porosity coefficient is chosen as $\xi = 0.1,\ 0.2$. Additionally, the nondimensional critical buckling load obtained for imperfect plates with porosity coefficient $\xi = 0.2$ is smaller than that for $\xi = 0.1$ regardless the porosity model.

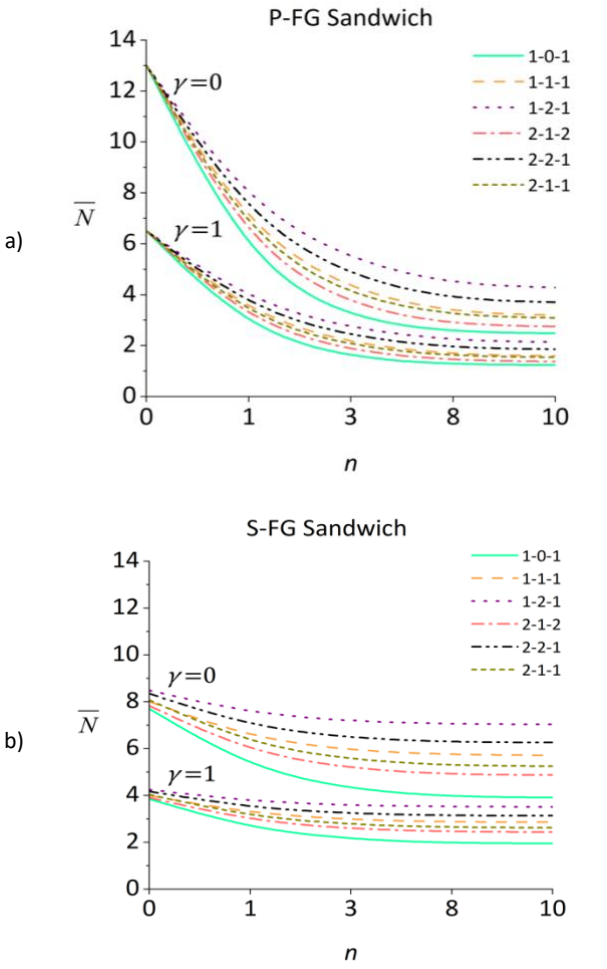

Figure 2. The variation of NDCBL of square a) P-FG and b) S-FG sandwich plates versus n (a/h = 10, γ = 0, 1)

In Figure 2, the variation of NDCBL of P-FG and S-FG sandwich plates versus the n using the present refined theory is shown. The increase of n reduces the critical buckling load values for all types of FG sandwich plates. For values of n > 5, the critical buckling load nearly remains constant. Note that P-FG and S-FG sandwich plates with 1–2–1 scheme shows higher NDCBLs compared to other FG sandwich schemes.

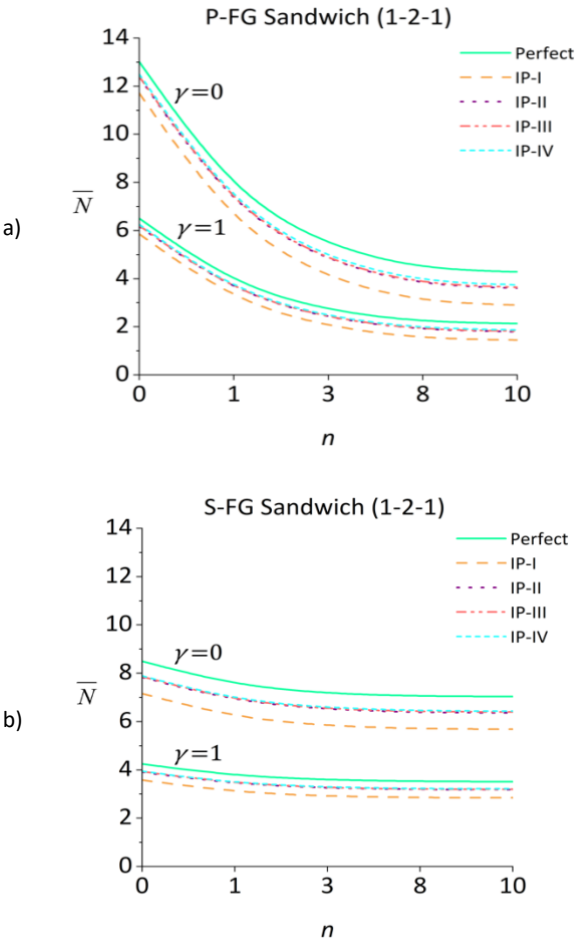

Figure 3. The variation of NDCBL of perfect and porous square a) P-FG, b) S-FG sandwich plate versus n (a/h = 10, ξ = 0.2)

The effects of n and porosity models on the NDCBLs of FG square sandwich plates are shown in Figure 3. The porosity coefficient is chosen as $\xi = 0.2$. The perfect FG plates have the highest NDCBL, while the IP-I FG plates have the lowest. Some similar results are obtained for IP-II and IP-III FG sandwiches. The n affects the critical buckling load of P-FG sandwich plates more than S-FG sandwich plates.

In Figure 4, the variation of NDCBLs versus the side-to-thickness ratio, a/h, for perfect and imperfect porous models are presented. The NDCBLs increase with increasing a/h. The critical buckling load values are highest for perfect FG plates, while lowest for the IP-I FG plates for all a/h ratios.

a)

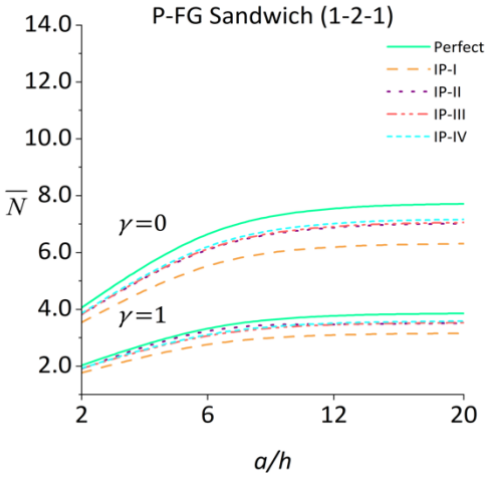

b)

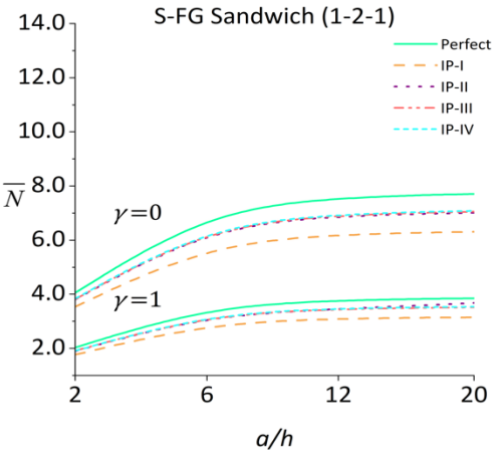

Figure 4. The variation of NDCBL of perfect and porous square a) P-FG, b) S-FG sandwich plate versus a/h (n = 1, ξ = 0.2)

8. Conclusion

This paper investigates the mechanical buckling behavior of porous FG sandwich plates using a refined shear deformation theory. Two types of FG sandwich plates, according to power-law and sigmoid-law were analyzed, considering four different porosity distribution types and accounting for both the material composition and sandwich plate scheme. Governing equations for simply supported FG sandwich plates are derived using the refined shear deformation plate theory, and closed-form solutions are obtained using Navier technique. The study examines the effects of porosity, sandwich plate geometry, and the inhomogeneity parameter on the buckling behavior of the FG sandwich plates. Key findings are summarized:

i. The results obtained using the current theory closely match those from previous ones.

ii. Increasing the volume fraction index reduces the non-dimensional critical buckling loads of FG sandwich plates.

iii. The side-to-thickness ratio significantly affects the critical buckling loads, where higher side-to-thickness ratios result higher non-dimensional critical buckling loads.

iv. Non-porous FG sandwich plates have the highest non-dimensional critical buckling loads which decrease with the increasing the porosity coefficient, regardless of the porosity distribution.

Declaration of Interest Statement

The authors declare that they have no competing financial interests or personal relationships that could have appeared to influence the work reported in this paper.

Acknowledgement

Present work received no financial grant in any form.

References

[1] Koizumi, M. (1993). The concept of FGM. *Ceramic Transactions, Functionally Gradient Materials*, *34*(1), 3–10.

[2] Suresh, S. & Mortensen, A. (1998). Fundamentals of Functionally Graded Materials, *IOM Communications*, London.

[3] Koizumi, M. (1997). FGM activities in Japan. *Composite Part B: Engineering*, *28*(1-2), 1–4. DOI: 10.1016/S1359-8368(96)00016-9

[4] Suresh, S. & Mortensen, A. (1997). Functionally graded metals and metal ceramic composites 2: thermomechanical behaviour. *International Materials Reviews*., *42*(3), 85–116. DOI: 10.1179/imr.1997.42.3.85

[5] Tanigawa, Y. (1995), Some basic thermoelastic problems for nonhomogeneous structural materials. *Applied. Mechanice Reviews*, *48*(6), 287–300.

[6] Cheng, Z. Q. & Batra, R. C. (2000), Exact correspondence between eigenvalues of membranes and functionally graded simply supported polygonal plates. *Journal of Sound and Vibration*, *229*(4), 879–895. DOI: 10.1006/jsvi.1999.2525

[7] Reddy, J. N. (2000). Analysis of functionally graded plates. *International Journal for Numerical Methods in Engineering*, *47*(1-3), 663–684.

[8] Praveen, G. V. & Reddy, J. N. (1998). Nonlinear transient thermoelastic analysis of functionally graded ceramic-metal plates. *International Journal of Solids and Structures*, *35*(33), 4457–4476. DOI:.1016/S0020-7683(97)00253-9

[9] Pan, E. & Han, F. (2005). Exact solution for functionally graded and layered magneto-electro-elastic plates. *International Journal of Engineering Science*, *43*(3-4), 321–339. DOI: 10.1016/j.ijengsci.2004.09.006

[10] Zhu, J., Lai, Z., Yin, Z., Jeon, J., & Lee, S. (2001), Fabrication of ZrO2–NiCr functionally graded material by powder metallurgy. Mater. Chem. Phys. *68*, 130–135. DOI: 10.1016/S0254-0584(00)00355-2

[11] Wattanasakulpong, N., Prusty, B.G., Kelly, D.W., & Hoffman, M.: (2012), Free vibration analysis of layered functionally graded beams with experimental validation. *Mater. Des.*, *36*, 182–190. DOI: 10.1016/j.matdes.2011.10.049

[12] Wattanasakulpong, N., Ungbhakorn, V. (2014). Linear and nonlinear vibration analysis of elastically restrained ends FGM beams with porosities. *Aerospace Science and Technology, 32*(1), 111–120. DOI: 10.1016/j.ast.2013.12.002.

[13] Ould Larbi, L., Saad, M., Zouatnia, N., Hadji, L., & Sayyad, A. S. (2024). A simple refined plate theory for buckling problems of in-plane bi-directional functionally graded plates with porosity under various boundary conditions. *Mechanics of Advanced Materials and Structures*, 1–10. DOI: 10.1080/15376494.2024.2346946.

[14] Draouche, K., Ait Amar Meziane, M., Hadji, L., Ait Atmane, H., Bennai, R., & Madan, R. (2024). Effect of porosity and boundary conditions on dynamic characteristics of cracked plates made of functionally graded materials. *Advances in Concrete Construction*, *18*(3), 2024, 175-190. DOI: 10.12989/acc.2024.18.3.175.

[15] Ait Atmane, H., Tounsi, A. & Bernard, F. Effect of thickness stretching and porosity on mechanical response of a functionally graded beams resting on elastic foundations. *Int J Mech Mater Des*, *13,* 71–84 (2017). DOI: 10.1007/s10999-015-9318-x.

[16] Ould Larbi, L., Saad, M., Zouatnia, N., Hadji, L., & Sayyad, A. S. (2024). A simple refined plate theory for buckling problems of in-plane bi-directional functionally graded plates with porosity under various boundary conditions. *Mechanics of Advanced Materials and Structures*, *32*(3), 403–412. DOI: 10.1080/15376494.2024.2346946.

[17] Nebab, M., Dahmane, M., Belqassim, A., Atmane, H. A., Bernard, F., Benadouda, & M., Hadji, L. (2023). Fundamental frequencies of cracked FGM beams with influence of porosity and Winkler/Pasternak/Kerr foundation support using a new quasi-3D HSDT. *Mechanics of Advanced Materials and Structures*, *31*(28), 10639–10651. DOI: 10.1080/15376494.2023.2294371

[18] Daikh, A.A. & Zenkour, A.M. (2019). Effect of porosity on the bending analysis of various functionally graded sandwich plates. *Mater. Res. Express*, *6*, 065703. DOI: 10.1088/2053-1591/ab0971

[19] Hadji, L., Ait Atmane, H., Tounsi, A., Mechab, I., & Adda Bedia, E.A. (2011), Free vibration of functionally graded sandwich plates using four-variable refined plate theory, *Appl. Math. Mech. -Engl. Ed*., *32*(7), 925–942 (2011). DOI: 10.1007/s10483-011-1470-9.

[20] Zenkour, A. M. (2005). A comprehensive analysis of functionally graded sandwich plates: Part 2—Buckling and free vibration. *International Journal of Solids and Structures*, *42*(18-19), 5243-5258. DOI: 10.1016/j.ijsolstr.2005.02.016.

[21] Daikh, A. A., & Zenkour, A. M. (2019). Free vibration and buckling of porous power-law and sigmoid functionally graded sandwich plates using a simple higher-order shear deformation theory. *Materials Research Express*, *6*(11), 115707. DOI: 10.1088/2053-1591/ab48a9

Table 1. Effects of volume fraction index on the non-dimensional biaxial buckling loads of an FG square sandwich plate ($\gamma = 1$, $a/h = 10$)

	n	Theory	1–0–1	1–1–1	1–2–1	2–1–2	2–2–1	2–1–1
P-FGM	0	Present	6,5028	6,5028	6,5028	6,5028	6,5028	6,5028
		Daikh et al. (2019 [21])	6,5027	6,5027	6,5027	6,5027	6,5027	6,5027
		SSDT (5 variable) [20]	6,5030	6,5030	6,5030	6,5030	6,5030	6,5030
		TSDT (5 variable) [20]	6,5025	6,5025	6,5025	6,5025	6,5025	6,5025
		FPT (5 variable) [20]	6,5022	6,5022	6,5022	6,5022	6,5022	6,5022
		CPT (3 variable)	6,8690	6,8690	6,8690	6,8690	6,8690	6,8690
	0,5	Present	3,6826	4,2184	4,6083	3,9708	4,4051	4,1125
		Daikh et al. (2019 [21])	3,6825	4,2184	4,6083	3,9707	4,4050	4,1125
		SSDT (5 variable) [20]	3,6828	4,2186	4,6084	3,9710	4,4052	4,1127
		TSDT (5 variable) [20]	3,6822	4,2182	4,6084	3,9704	4,4050	4,1124
		FPT (5 variable) [20]	3,6687	4,2052	4,5976	3,9566	4,3934	4,1001
		CPT (3 variable)	3,8270	4,3903	4,8076	4,1280	4,5913	4,2811
	1	Present	2,5840	3,2326	3,7532	2,9204	3,4748	3,0972
		Daikh et al. (2019 [21])	2,5839	3,2325	3,7532	2,9203	3,4748	3,0971
		SSDT (5 variable) [20]	2,5842	3,2327	3,7531	2,9206	3,4749	3,0973
		TSDT (5 variable) [20]	2,5836	3,2324	3,7533	2,9200	3,4747	3,0970
		FPT (5 variable) [20]	2,5712	3,2195	3,7418	2,9069	3,4629	3,0851
		CPT (3 variable)	2,6662	3,3408	3,8920	3,0137	3,5983	3,2020
	5	Present	1,3298	1,7902	2,3674	1,5218	2,0563	1,7021
		Daikh et al. (2019 [21])	1,3296	1,7901	2,3674	1,5217	2,0563	1,7020
		SSDT (5 variable) [20]	1,3300	1,7903	2,3674	1,5220	2,0564	1,7022
		TSDT (5 variable) [20]	1,3291	1,7898	2,3673	1,5213	2,0561	1,7018
		FPT (5 variable) [20]	1,3192	1,7798	2,3574	1,5113	2,0464	1,6927
		CPT (3 variable)	1,3654	1,8287	2,4286	1,5535	2,1062	1,7421
S-FGM	0	Present	3,8503	4,0053	4,2453	3,9135	4,1732	4,0357
		Daikh et al. (2019 [21])	3,8506	4,0062	4,2459	3,9144	4,1739	4,0363
		SSDT (5 variable) [20]	3,8505	4,0060	4,2457	3,9142	4,1737	4,0361
		TSDT (5 variable) [20]	3,8502	4,0037	4,2443	3,9119	4,1722	4,0349
		FPT (5 variable) [20]	3,8500	3,9836	4,2249	3,8954	4,1553	4,0220
		CPT (3 variable)	4,0671	4,1709	4,4174	4,0896	4,3519	4,2230
	0,5	Present	2,9728	3,4660	3,9012	3,2218	3,6870	3,3856
		Daikh et al. (2019 [21])	2,9732	3,4664	3,9014	3,2223	3,6873	3,3858
		SSDT (5 variable) [20]	2,9731	3,4662	3,9014	3,2221	3,6872	3,3858
		TSDT (5 variable) [20]	2,9723	3,4654	3,9011	3,2211	3,6867	3,3852
		FPT (5 variable) [20]	2,9598	3,4501	3,8873	3,2061	3,6731	3,3722
		CPT (3 variable)	3,0865	3,5898	4,0496	3,3364	3,8259	3,5123
	1	Present	2,5840	3,2326	3,7531	2,9204	3,4748	3,0972
		Daikh et al. (2019 [21])	2,5839	3,2325	3,7532	2,9203	3,4748	3,0971
		SSDT (5 variable) [20]	2,5842	3,2327	3,7531	2,9206	3,4749	3,0973
		TSDT (5 variable) [20]	2,5836	3,2324	3,7533	2,9200	3,4747	3,0970
		FPT (5 variable) [20]	2,5712	3,2195	3,7418	2,9069	3,4629	3,0851
		CPT (3 variable)	2,6662	3,3408	3,8920	3,0137	3,5983	3,2020
	5	Present	2,0187	2,8972	3,5411	2,4856	3,1679	2,6757
		Daikh et al. (2019 [21])	2,0189	2,8971	3,5408	2,4856	3,1679	2,6758
		SSDT (5 variable) [20]	2,0188	2,8971	3,5409	2,4856	3,1679	2,6758
		TSDT (5 variable) [20]	2,0184	2,8974	3,5416	2,4856	3,1681	2,6757
		FPT (5 variable) [20]	2,0083	2,8878	3,5333	2,4756	3,1586	2,6658
		CPT (3 variable)	2,0659	2,9850	3,6669	2,5526	3,2709	2,7526

Table 2. Effects of porosity on the non-dimensional frequencies of FG square sandwich plate ($a/h = 10$, $n = 2$)

	Porosity	ξ	1–0–1	1–1–1	1–2–1	2–1–2	2–2–1	2–1–1
P-FGM	Perfect	0	1.7787	2.4046	2.9934	2.0824	2.6734	2.2704
	Imperfect I	0,1	1.3867	2.0290	2.6549	1.6941	2.3046	1.8787
		0,2	0.9930	1.6516	2.3147	1.3039	1.9296	1.4795
	Imperfect II	0,1	1.6077	2.2246	2.8275	1.9014	2.4969	2.0894
		0,2	1.4364	2.0441	2.6613	1.7199	2.3191	1.9069
	Imperfect III	0,1	1.6118	2.2289	2.8315	1.9058	2.5013	2.0939
		0,2	1.4525	2.0611	2.6770	1.7370	2.3359	1.9241
	Imperfect IV	0,1	1.6793	2.2747	2.8607	1.9631	2.5436	2.1496
		0,2	1.5799	2.1446	2.7278	1.8438	2.4131	2.0283
S-FGM	Perfect	0	2.2554	3.0372	3.6295	2.6673	3.2963	2.8526
	Imperfect I	0,1	1.8637	2.6643	3.2937	2.2810	2.9358	2.4689
		0,2	1.4706	2.2898	2.9565	1.8931	2.5707	2.0798
	Imperfect II	0,1	2.0659	2.8528	3.4626	2.4775	3.1184	2.6648
		0,2	1.8761	2.6680	3.2953	2.2874	2.9394	2.4759
	Imperfect III	0,1	2.0705	2.8572	3.4666	2.4821	3.1227	2.6694
		0,2	1.8939	2.6854	3.3111	2.3053	2.9562	2.4936
	Imperfect IV	0,1	2.1081	2.8795	3.4798	2.5115	3.1429	2.6976
		0,2	1.9607	2.7216	3.3299	2.3555	2.9888	2.5420

Research Article

JOURNAL OF CERAMICS AND COMPOSITES

e-ISSN: 3062-293X

Performance prediction of pavement structures using non-destructive deflection testing and backcalculation

Betul Nerkiz[a,*], Kemal Armagan[b]

[a]Department of Civil Engineering, Faculty of Engineering, Karamanoğlu Mehmetbey University, Türkiye
[b]Department of Civil Engineering, Faculty of Engineering, Karamanoğlu Mehmetbey University, Türkiye

Highlights

- Sustainable transportation – durable pavement structures
- Non-destructive testing – fast and reliable data acquisition
- Backcalculation – performance-oriented analysis

Abstract

Highway pavement plays a critical role in the economic development of cities and nations, and with proper design and maintenance, it supports sustainable transportation. Performance prediction models help evaluate the efficiency and durability of the road network, assisting in the development of strategies for infrastructure improvements. These predictions are made using computer-aided modeling and simulation techniques, aiming to identify future maintenance needs. Non-destructive testing (NDT) methods are used to assess the condition of existing roadways and provide information about their physical state. These techniques are vital for preserving pavement performance and enhancing traffic safety. NDT methods typically do not damage the materials being tested, and results can be obtained quickly, enabling efficient road maintenance management. Backcalculation problems involve analyzing data obtained from methods such as deflection testing to determine the mechanical properties of pavement structures. These methods play a significant role in enhancing the sustainability and safety of highway networks and contribute to the effective management of roadway maintenance. In this study, the performance prediction of pavement structures is investigated through backcalculation using data obtained from non-destructive deflection testing.

Information

Received:
19.01.2025
Received in revised:
10.03.2025
Accepted:
17.03.2025

Keywords: *Non-Destructive Deflection Testing, backcalculation method, performance prediction*

1. Introduction

Asphalt is a composite material extensively utilized in road engineering, consisting of a bitumen binder and mineral aggregates combined in defined proportions. As a multiphase and structurally heterogeneous material, asphalt exemplifies the foundational concept of composite materials: the integration of components with differing physical or chemical properties to produce a material with enhanced performance characteristics compared to its individual constituents [1]. In asphalt, bitumen imparts elasticity and flexibility, while mineral aggregates contribute stiffness and load-bearing capacity. The interaction between these two phases governs critical performance attributes such as fatigue resistance, deformation behavior, and temperature sensitivity [2,3].

The performance of asphalt can be further optimized through the incorporation of additives such as polymers, fibers, and nanomaterials, which enhance its thermal stability and long-term durability [4,5]. Moreover, the use of recycled materials including reclaimed asphalt pavement (RAP) and plastic waste contributes not only to economic efficiency but also to environmental sustainability by promoting circular material use [6].

Pavement structures are typically constructed as multilayered systems comprising subgrade, sub-base, base, and surface layers. These layers function collectively to distribute traffic loads and must be engineered to perform reliably under diverse climatic and loading conditions. Pavements are generally classified into three categories: flexible, rigid, and composite [7]. Flexible pavements, primarily composed of asphalt layers, are cost-effective, easy to construct, and relatively simple to

*Corresponding author: betulnerkiz381@gmail.com (B., Nerkiz), 05339403319

maintain, though they may be less suitable for heavy traffic. In contrast, rigid pavements, typically made of concrete slabs, offer superior durability and load distribution capacity but entail higher construction and maintenance costs. Composite pavements integrate characteristics of both types, providing a balanced approach by enhancing structural performance while maintaining a reasonable cost profile [7].

Highway pavements represent a fundamental component of transportation infrastructure, enabling safe and efficient mobility for vehicles, cyclists, and pedestrians. In addition to supporting mobility, they play a strategic role in urban and national economic development. When integrated with essential infrastructure elements such as road markings, lighting, and traffic control systems, well-designed pavements contribute significantly to road safety, efficiency, and sustainability [8].

To ensure long-term performance and optimize resource allocation, pavement performance prediction has emerged as a key tool in infrastructure management. Computer-aided modeling and simulation techniques allow for the evaluation of pavement behavior under traffic loading, aging processes, and environmental influences. These models assist engineers and planners in identifying future maintenance needs, anticipating structural deficiencies, and assessing the impacts of climate change on pavement systems [9].

In this context, composite pavements offer a particularly effective solution by combining the structural advantages of rigid pavements with the adaptability and smoothness of flexible surfaces. They are especially suitable for regions with weak subgrades and varying traffic demands, offering a cost-effective yet durable alternative for long-term infrastructure needs [10].

Non-Destructive Testing (NDT) methods have become indispensable in modern pavement evaluation. These in-situ techniques enable the assessment of subsurface deformation and structural integrity without compromising the pavement material. By employing surface sensors and real-time data collection, NDT facilitates periodic monitoring of pavement conditions, thereby informing proactive maintenance strategies [11]. Compared to conventional laboratory testing, NDT is faster, more economical, and allows for broader spatial assessment. This is particularly valuable for aging highway networks constructed in the 1960s and 1970s, many of which are nearing or exceeding their design lifespans. By offering detailed insights into existing conditions, NDT supports more efficient resource use and maintenance planning [12].

2. Performance Prediction of Pavement Structures Using Back calculation from NDT

Pavements are fundamental infrastructure components that ensure user comfort and safety. Accurate forecasting of future conditions allows for proper budget planning for maintenance activities. The evaluation of pavement performance involves detailed analysis and is directly related to ride quality and serviceability. Serviceability, which reflects this relationship, considers both the riding comfort and the pavement's ability to provide service as seen in Figure 1. Overall, pavement performance is commonly associated with driver satisfaction [13].

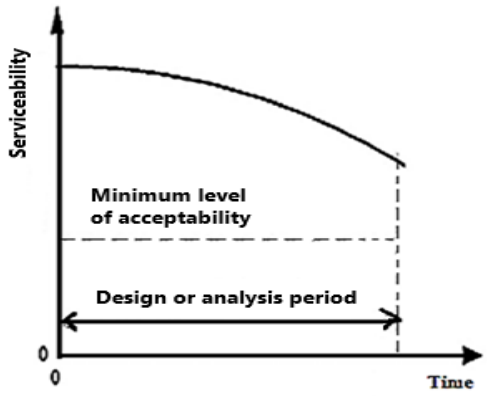

Figure 1. Serviceability degradation [14]

To evaluate the performance of pavement structures, detailed section-level analysis is required. This analysis includes ride quality and traffic data over a specific time period. Pavements are assessed based on user satisfaction or dissatisfaction in terms of ride quality, and the outcomes of these assessments inform decisions regarding maintenance, rehabilitation, or reconstruction.

Various methods have been developed for evaluating structural capacity, which require measurements to estimate the pavement's load-carrying ability and service life. The results of these structural assessments can be used to design improvement projects. Among both destructive and non-destructive structural evaluation methods, deflection measurement techniques are widely used.

Non-destructive techniques are generally preferred due to their lower cost, minimal traffic disruption, and reduced impact on the pavement structure. However, deflection measurements require appropriate equipment and skilled personnel, making structural evaluation a costly process. Therefore, a carefully planned strategy is necessary for effective structural assessment. The structural capacity of pavements can be evaluated non-destructively using various deflection measurement devices. These devices assess the structural response of pavements based on different methods [14].

Highways are the most commonly used mode of transportation worldwide and are designed to function

with a certain degree of flexibility over time. However, environmental conditions and mechanical loading can lead to degradation of pavement structures. These deteriorations not only affect traffic safety but also lead to significant economic losses. Efforts to assess pavement performance are carried out within the framework of Pavement Management Systems (PMS) through models such as the Present Serviceability Index (PSI), Pavement Condition Index (PCI), and International Roughness Index (IRI). These models aim to monitor pavement service levels and enable timely interventions [15].

Performance modeling significantly impacts the lifespan, design, and financial aspects of pavement management systems. It constitutes an essential part of analyses conducted both at the network and project levels. Accurately determining pavement performance and deterioration prediction is crucial for maintaining road performance, keeping in mind that progressive deterioration can increase costs over time. Since future conditions cannot be precisely predicted, performance curves are used for estimations at specific points in time. A typical performance curve indicates the timing of maintenance and rehabilitation based on anticipated future pavement deterioration. Specific criteria must be established to compare predicted performance with actual measurements, which are generally based on standards and specifications. The information required to develop prediction models includes databases (such as construction date, IRI value, PSI, RN, AADT, etc.), parameters affecting deterioration, appropriate model selection, and defining certain criteria. Thus, with a suitable database and defined benchmarks, prediction models for pavements can be developed [16].

The existence of systems to manage urban pavements is inevitable. The most challenging step of these systems is to determine the current performance of the pavements. Existing performance can be quantitatively expressed through various techniques and indices, although these methods may require substantial infrastructure investment. In national road networks, pavement performance is generally assessed by device-based measurements. These measurements commonly use the International Roughness Index (IRI). Additionally, deflection data are preferred in pavement evaluations. Researchers often compare surface distress and/or roughness data with vehicle vertical vibration data to determine the current pavement performance [17].

Pavement performance refers to the ability of the pavement to provide ride comfort and safety over time. Performance evaluation requires data on surface characteristics and structural strength. Pavement characteristics are defined as physical properties, including surface type, smoothness, texture, and skid resistance. Pavement performance assessments are conducted by comprehensively evaluating criteria such as ride comfort, safety, surface integrity, structural adequacy, and surface distresses. These evaluations are typically based on pavement management system reports [18].

In recent years, the use of NDT methods has increased significantly in construction and environmental engineering applications. Research into electrical, electromagnetic, optical, and acoustic NDT techniques has accelerated. The potential of these methods has been extensively investigated, and they are widely used across many fields [19].

Continuous monitoring of the pavement network plays an important role in determining the structural performance. In this monitoring process, deflection measurements are commonly used to assess structural capacity. The Non-Destructive Deflection Test is the most widespread method for determining pavement structural condition and detecting variable parameters of the pavement structure. Results from this test help identify the properties of pavement layers. Unlike destructive testing, the Non-Destructive Deflection Test is performed without stopping traffic or damaging the pavement, making it one of the most reliable methods. The simple and fast falling weight deflectometer used in NDT is widely applied to both flexible and rigid pavements [20].

NDT methods are employed to assess existing pavement structures without necessitating subsequent repairs. These methods have two main advantages over destructive testing: first, they allow in-situ evaluation without causing damage or alteration to the materials. Destructive methods may damage underlying layers and require laboratory conditions. Second, non-destructive methods enable faster, more economical testing with less traffic disruption, allowing for a greater number of measurements. These methods are preferred to minimize traffic interruptions and to identify areas for laboratory sample collection for further material property evaluation. The focus is on determining the need for destructive testing, the location of such testing, and on-site measurement of current pavement structural conditions. These methods can assess structural or functional conditions. While data collected by non-destructive methods are objective, data analysis and interpretation may be subjective. Examples include Falling Weight Deflectometer, Dynamic Cone Penetrometer (DCP), Ground Penetrating Radar, and Seismic Method Devices [21].

Figure 2. Falling weight deflectometer [22]

The Falling Weight Deflectometer (FWD) is a device used for evaluating pavement structures. This device which is seen in Figure 2 applies a transient load to the pavement and measures the deflection values that occur under this load. This method is utilized to determine the mechanical properties of the pavement through back-calculation techniques. The DCP is a method used to measure soil strength is seen in Figure 3. However, it can also be employed to identify sudden changes in strength within pavement layers and to measure layer thickness. Ground Penetrating Radar (GPR) seen in Figure 4, is a non-destructive technique used to investigate the composition and extent of materials. It is also used to determine layer thicknesses of various pavements and to explore subsurface areas. Its high-speed data collection capability reduces traffic control needs and enhances safety. The Spectral Analysis of Surface Waves (SASW) method is used to evaluate pavement systems from a seismic perspective. This technique analyzes the travel time and response of Rayleigh waves to determine material properties [23].

These methods enable the integration of experimental approaches that can be used for the evaluation and performance monitoring of pavement structures. One of the NDT methods, the DCP, can determine layer strength without excavation. Similarly, the Lightweight Deflectometer (LWD) is another method used to assess the structural properties and performance of pavement structures [24].

Ground Penetrating Radar test is used to estimate asphalt concrete properties, while density and thickness measurements are performed with the Falling Weight Deflectometer test to assess the elastic modulus and estimate elastic properties using Ultrasonic Pulse Velocity (UPV). A small error and good correlation can be found between NDT methods and standard tests. NDT methods can be repeated numerous times, and with the latest software, surface, subsurface, and volumetric indicators can be detected more quickly and at relatively lower costs.

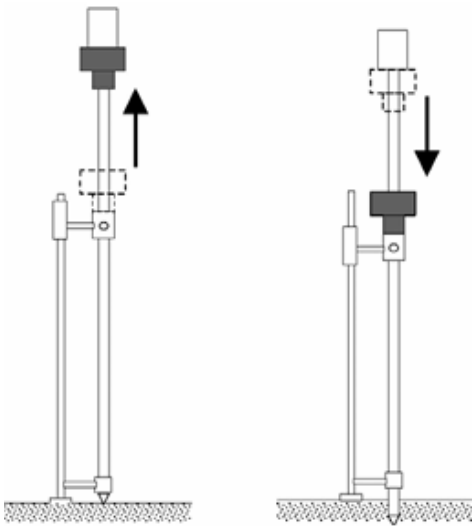

Figure 3. Dynamic cone penetrometer [25]

Figure 4. Ground penetrating radar [27]

In highway transportation, the use of innovative NDT methods for in-situ evaluation of pavement structures is increasing. GPR is a geophysical positioning technique that uses radio waves to capture subsurface images in a minimally invasive manner. It is also used to locate structural objects and evaluate pavement materials, layer thickness, and pavement characteristics.

The Falling Weight Deflectometer is an NDT method that measures the vertical deflection response of pavement layers. Its use is widespread in the pavement design industry for identifying weak pavement areas, back-calculating layer properties, and estimating the remaining service life of the structure. The FWD simulates the effects of wheel loads on concrete by generating impact forces from various drop heights, and geophones and seismometers are commonly used on transducers for various applications following loading [20,26].

A reliable measurement method is necessary to determine the effects of traffic and environmental conditions on pavement structures over time. For this purpose, the Falling Weight Deflectometer or more complex Traffic Speed Deflection Devices can be used as seen in Figure 5. Although FWD is an important tool for structural evaluation, thickness data are also critical as they are required for strain analysis and pavement rehabilitation. In particular, FWD deflections, evaluated together with pavement layer thicknesses, allow for the analysis of the mechanical responses of the pavement, enabling the condition of the pavement to be assessed both individually and overall [28].

NDT aims to determine the physical integrity and quality of the element while preventing deformation. NDT methods can be applied under various conditions based on different physical principles. These methods are faster than destructive techniques and are widely used across many fields. NDT applications can be conducted without interrupting operational processes, and results are generally obtained immediately. Selecting the most appropriate method for testing material safety is crucial and should be done considering various factors [29].

The structural condition of pavement can be determined non-destructively using the FWD. The FWD operates on the principle of transient loading and evaluates the load-carrying capacity of the pavement. In these devices, the force is generated by a guided mass and transmitted to the pavement as an impact load resembling a half-sine wave. Loading is applied within a specific time interval and frequency. The impact effect of the FWD is very close to the effect of standard axle loads, and it provides more reliable results than other NDT methods.

Due to temperature-dependent changes in flexible pavements, the measured deflection values may need to be corrected according to a reference temperature value for accurate evaluation. In flexible pavement systems, the durability of bituminous hot mix (BHM) layers varies depending on factors such as temperature, loading duration, and load magnitude. It should be noted that during deflection measurements, the pavement temperature is an important parameter to monitor. Since the stiffness of asphalt layers changes with temperature, changes in pavement temperature affect the deflections. At higher temperatures, asphalt stiffness decreases, causing deflections to increase [30].

Figure 5. Deflection measurement [11]

NDT utilizes various data acquisition devices and analysis methods. These data are generally used to assess the structural or functional condition of a pavement. Engineers can calculate the strength of pavement layers by using deflection basin data obtained from flexible pavements and rigid center NDT tests. This analysis method is commonly referred to as back calculation because engineers typically perform the inverse of traditional pavement design. Instead of determining the thickness of each pavement layer, back calculation generally solves for the pavement layer moduli based on assumed uniform layer thicknesses.

NDT encompasses various measurement and analysis techniques used to evaluate the current condition of structural materials or components. This method allows examination without altering the composition or shape of the material. In recent years, especially in the fields of civil and mechanical engineering, there has been increasing interest in damage-free methods used to detect defects in materials [31-33].

There are several models for estimating the remaining service life of Bituminous Hot Mix (BHM) pavements. These models are based on NDT methods that utilize material properties. The structural condition of the pavement depends on factors such as the structural capacity of the superstructure, layer thickness, and material properties. A widely used method to determine the structural condition of highway pavements involves measuring surface deflections of the pavement with a NDT device. These data are essential for determining the elastic parameters of pavement layers. To calculate elastic moduli, the parameters affecting deflection values must be known, and the relationship between these parameters and deflection must be established; this process is called back calculation. Deflection measurements provide information about the current condition of the pavement and are important for understanding the relationship between material properties and pavement performance. Data obtained from NDT devices help determine the elastic parameters of pavement layers. However, in addition to deflection tests, data interpretation and analysis are critical and these analyses can be used to identify pavement material properties [11,19,30,34].

NDT methods are generally preferred for evaluating the performance of flexible pavements. Among these methods, the Falling Weight Deflectometer (FWD) technique is the most commonly used. Using this method, time-dependent deflection values caused by applied loads are measured at multiple points along the pavement. Performance evaluation of flexible pavements is typically conducted for two main purposes: to provide information about the physical condition of the existing pavement and to verify the quality of newly constructed pavement layers.

NDT methods are widely preferred for determining mechanical properties because they do not damage the pavement and provide rapid results. Using these methods, the material properties of the pavement layers can be measured at low strain levels. Back calculation problems are considered optimization problems aiming to identify the best model parameters that correspond to known input-output data.

The back calculation process involves the mechanical analysis of surface deflections measured by deflectometers. This process consists of two parts: forward analysis and error correction algorithm. The forward analysis computes deflections, while the error correction algorithm calculates errors and updates the modulus estimates.

For back calculation to be successful, the forward computation model must produce accurate results, as system performance depends on the accuracy of the input and output data used [29,33,35].

To achieve reliable results, a comprehensive analysis of all influencing factors is essential. Factors such as sensor configuration, base layer properties, connection spacing, and temperature conditions must be taken into account when interpreting backcalculation outcomes. The measerement point accuracy as seen in Figure 6 and the distance between the sensors in FWD is also important in backcalculation. For rigid pavements, slab curling has been identified as a critical factor affecting FWD deflection measurements; therefore, its impact should be considered during the interpretation of backcalculation results.

Figure 6. Placement of the falling weight deflectometer on the measurement point [12]

Various backcalculation methods exist for determining base and subgrade moduli or subgrade reaction coefficients (k) in rigid pavements, each possessing distinct strengths and limitations. Inconsistencies among these methods have been recognized as a significant source of variation. Backcalculation procedures typically require the modular ratio as an input parameter, which should be established based on engineering judgment.

Backcalculated parameters for each deflection basin are compared against corresponding average values. If a backcalculated parameter deviates from the average by more than two standard deviations, an appropriate flag is raised. The primary goal of including the base layer in the backcalculation analysis is to account for its structural contribution to the overall pavement stiffness [36,37].

Accurately predicting the remaining service life of existing flexible pavements can lead to substantial savings in maintenance and rehabilitation costs. Backcalculation of structural capacity from non-destructive test data provides an efficient and cost-effective approach. Deflection data obtained from FWD tests are used to estimate the mechanical properties of pavement layers. However, backcalculation algorithms can influence the results, and many highway agencies worldwide still employ simplified methods.

An iterative procedure is typically employed for estimating pavement layer moduli through backcalculation. NDT facilitates the application of a mechanical approach in pavement design and rehabilitation by measuring in-situ material properties using appropriate techniques [38].

In flexible pavement systems, the backcalculation problem primarily involves determining the elastic modulus of individual layers as seen in Figure 7. Within these computational algorithms, the layer thicknesses and Poisson's ratio are considered known parameters. Initially, an elastic modulus value is assigned to each layer. A forward calculation is then performed using these values, and the computed deformation values are compared to the measured data. If the difference exceeds a specified tolerance, the elastic moduli are adjusted and the process repeats iteratively until the results fall within the acceptable tolerance. The initial guesses for elastic moduli significantly affect the convergence rate of the backcalculation procedure. The accuracy of the derived elastic moduli depends on the reliability of known pavement properties, and the goal is to minimize the discrepancy between measured and calculated deformations within a defined tolerance [40,41].

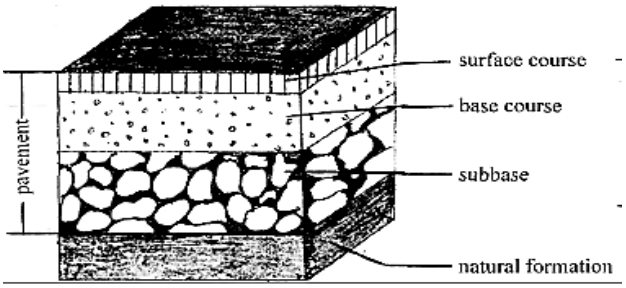

Figure 7. Layers in flexible pavements [39]

In summary, backcalculation is a widely used technique in engineering and materials science. This approach typically involves utilizing experimental data to infer material or structural properties. For instance, data obtained from experimental tests on a structure or material are analyzed via backcalculation algorithms. Through this analysis, structural parameters or material characteristics such as elastic modulus, strength, or thermal conductivity can be determined. Backcalculation is particularly valuable in complex structural systems or materials where direct measurement is challenging [42]. It facilitates understanding and predicting material behavior by analyzing experimental results. Additionally, backcalculation is extensively applied in engineering design and optimization processes, as the insights gained enhance the robustness and evidence-based nature of decision-making.

3. Conclusion

This study focuses on NDT methods employed for evaluating pavement performance. It highlights the significance of NDT approaches and explains how these methods are implemented through various techniques. The non-invasive nature of these tests offers numerous advantages for pavement assessment and performance monitoring. The importance of NDT methods in construction and pavement engineering fields is emphasized.

Among NDT techniques, the Falling Weight Deflectometer is one of the preferred methods for assessing the performance of flexible pavements. The results section underlines the crucial role of NDT methods in effectively evaluating pavement performance. Furthermore, the potential of these methods for future research and practical applications is acknowledged. Ultimately, NDT methods are identified as vital tools for ensuring the safety, durability, and sustainability of pavement structures, and their effective utilization is considered an essential requirement for pavement infrastructure management.

Backcalculation refers to an analytical approach used to determine structural or material properties by processing experimental data in a reverse manner. For example, to identify the elastic characteristics of a material, different loads are applied and the resulting deformations are measured. These experimental measurements are then processed through backcalculation algorithms to estimate properties such as the elastic modulus. This method is particularly useful in cases where direct measurements are difficult, providing a computational means to understand and predict material behavior based on empirical data.

References

[1] Yalcin, B. F., Bakir, E., Yalcin, E., Yilmaz, M. (2024). Composite Modifiers to Improve The Rheological Properties of Asphalt Binders. Journal of Materials in Civil Engineering, 36(6). https://doi.org/10.1061/JMCEE7.MTENG-17524

[2] Mallick, R. B., El-Korchi, T. (2017). Pavement Engineering: Principles and Practice (3rd ed.). CRC Press.

[3] Read, J., Whiteoak, D. (2003). The Shell Bitumen Handbook (5th ed.). Thomas Telford Publishing

[4] Yildirim, Y. (2007). Polymer Modified Asphalt Binders. Construction and Building Materials, 21(1), 66–72. https://doi.org/10.1016/j. conbuildmat.2005.07.007

[5] Alas, M., Albrka, A., Gökçekuş, H. (2022). The High Temperature Performance Evaluation of Polymer/Nanocomposite Modified Asphalt Cement. Teknik Dergi, 33(4), 12143–12162.

[6] Zaumanis, M., Mallick, R. B., Frank, R. (2020). Sustainable Asphalt Pavements: Technologies, Knowledge Gaps and Opportunities. Springer.

[7] Kaşak S., Komut M., (2019). Karayolları Beton Yol Üstyapılar Projelendirme Rehberi, Ulaştırma ve Altyapı Bakanlığı Karayolları Genel Müdürlüğü, Ankara.

[8] Bağdatli M. E. C., (2010), Esnek Üstyapı Kaplamalarındaki Hasar Özelliklerinin Bakım Maliyetleri Üzerine Etkisi, Namık Kemal Üniversitesi Yüksek Lisans Tezi, Tekirdağ.

[9] Kırbaş U., (2018). Karaşahin M., Şehiriçi Yollarda Üstyapıların Mevcut Performansını Belirlemek İçin Bir Yöntem, Teknik Dergi, 8459-8467, Yazı 507, Teknik Not.

[10] Geçkil T., Tanyıldızı M. M., (2019). Zemin Taşıma Gücünün Rijit ve Esnek Üstyapıların Kalınlıklarına ve Maliyetlerine Etkisi, Fırat Üniversitesi Müh. Bil. Dergisi, 31(2), 399-406.

[11] Erkmen F., Kalyoncuoglu F., (2023). Düşen Ağırlıklı Deflektometre Ölçümlerinde Asfalt Sıcaklığı Etkisi, Süleyman Demirel Üniversitesi Fen Bilimleri Enstitüsü Dergisi, 27:284–90. https://doi.org/10.19113/sdufenbed.1220320

[12] Ellis T., (2008). ScholarWorks@UARK A Comparison of Nondestructive Testing Backcalculation Techniques for Rigid and Flexible Pavements.

[13] Kırbaş U., (2013). İstanbul Şehiriçi Yollarda Üstyapı Bakım Yönetim Sistemi Kurulması, Türkiye Örneği, İstanbul Üniversitesi Fen Bilimleri Enstitüsü, Aralık.

[14] Kırbaş U., Karaşahin M., (2015). Şehiriçi Bitümlü Sıcak Karışım Kaplamalı Yollarda İklim ve Üstyapı Yaşına Endeksli Bir Üstyapı Bozulma Tahmin Modeli Geliştirilmesi, Volume: 11 Issue: 2, 10 - 19.

[15] Yarcı Ş., (2021). Karayolu Esnek Üstaypılarında Termal Alan Yöntemi ile Performans Tahmini, Afyon Kocatepe Üniversitesi, Fen Bilimleri Üniversitesi Yüksek Lisans Tezi, Temmuz.

[16] Kırbaş U., Karaşahin M., (2018). A Method For Determining Existing Pavement Performance in Urban Roads, Teknik Dergi/Technical Journal of Turkish Chamber of Civil Engineers, 29:8459–67. https://doi.org/10.18400/tekderg.373899

[17] Hergüner A. T., (2009). Türkiye Otoyol Ağı İçin Üstyapı Yönetim Sistemi, İstanbul Teknik Üniversitesi Fen Bilimleri Enstitüsü, Doktora Tezi, Temmuz.

[18] Çarkanat F., Bozatlı S., Abut Y., (2022). Esnek Üstyapılarda Kalıcı Deformasyon Ve Yorulmaya Bağlı Mekanistik Bir Modelleme Ve Duyarlılık Analizi, Konya Mühendislik Bilimleri Dergisi, C. 10, S. 2, 512-523.

[19] Tosti F., Benedetto A., Ciampoli L. B., D'Amico F., Plati C., Loizos A., (2020). Guest Editorial: Data Fusion, Integration and Advances of Non-Destructive Testing Methods in Civil and Environmental Engineering, NDT and E International, 115.

[20] Kamruzaman N., Hidayah N., Kamaruddin M., (2021). Non-Destructive Method for Asphalt Pavement Evaluation: A Review, Recent Trends in Civil Engineering and Built Environment, 2:315–22.

[21] Serin S., (2014). Tahribatsız Test Yöntemleri İle Esnek Üstyapıların Fiziksel Ve Mekanik Özelliklerinin Modellenmesi, Süleyman Demirel Üniversitesi Doktora Tezi.

[22] Domitrović J., Rukavina T., (2013). Application of GPR and FWD in assessing pavement bearing capacity. Article No.2, Romanian Journal of Transport Infrastructure, Vol.2, 2013, No.2 DOI: 10.1515/rjti-2015-0015

[23] Bayazıt M., (2019). Karayolu Üstyapısında Tahribatsız Elektromanyetik Test Yöntemi İle Kalite Kontrol, Düzce Üniversitesi Yüksek Lisans Tezi.

[24] Sarıoğlu O., Saltan M., (2021). Sathi Kaplamalı Yolların Yapısal Performansının Değerlendirilmesi, Mühendislik Bilimleri ve Tasarım Dergisi, 9:463-75.

[25] Uz V. E., Saltan M., (2012). Granüler Yol Tabakalarının Yerinde Değerlendirme Yöntemleri: Dinamik Koni Penetrometre (DCP) Testi, SDU International Technologic Science, Vol. 4, No 2, pp. 70-88.

[26] Plati C., Loizos A., Gkyrtis K., (2020). Integration of Non-Destructive Testing Methods to Assess Asphalt Pavement Thickness, NDT and E International, 115.

[27] Aydın A., (2023). Yer Radarı Yöntemi İle Kayıp Alt Yapı Şebekelerinin Tespiti (Giresun İli Örneği), Avrasya Üniversitesi Yüksek Lisans Tezi.

[28] FAA., (2011). Airports Engineering Division AAS., 150/5370-11B, Use of Nondestructive Testing in the Evaluation of Airport Pavements, 30 September.

[29] Kara O., Erdal H., Çelik H. H., (2007). Tahribatsız Test Yöntemleri: Karşılaştırmalı Bir Derleme Çalışması,

Marmara Fen Bilimleri Dergisi. https://doi.org/10.7240/marufbd.326674

[30] Gürcan T., (2019). Atık Asfalt Kaplamalarla Oluşturulmuş Bitümlü Sıcak Karışım Özelliklerinin İleri Düzey Performans Deneyleriyle Belirlenmesi, Akdeniz Üniversitesi Yüksek Lisans Tezi, Temmuz.

[31] Lee S. Y., Choi J. S., Le T. H. M., (2024). Unraveling The Optimal Strategies for Asphalt Pavement Longevity Through Preventive Maintenance: A Case Study in South Korea, Case Studies in Construction Materials.

[32] Rucka M., (2020). Special Issue: "Non-Destructive Testing of Structures." Materials, 13:1-6

[33] Lav A. H., Göktepe A. B., Ağar E., (2005). Esnek Üstyapılarda Mekanik Özelliklerin Yapay Sinir Ağları Kullanılarak Geri-Hesaplanması, İ.T.Ü. Dergisi/d Mühendislik Cilt:4, Sayı:2, 31-42, Nisan.

[34] Saltan M., Alaefary F., (2018). Anfıs Yönteminin Esnek Yol Üstaypılarının Yapısal Analizinde Kullanılabilirliği, Mühendislik Bilimleri ve Tasarım Dergisi, 6:396–405.

[35] Saltan M., Karaşahin M., (2016). A Finite Element Based Backcalculation Program for Flexible Pavements, Indian Journal of Engineering and Materials Sciences 13(3):221-230.

[36] Khazanovich L., Tayabji S., Darter M., (2001). Backcalculation of Layer Parameters for LTPP Test Sections, Volume I: Slab on Elastic Solid and Slab on Dense-Liquid Foundation Analysis of Rigid Pavements, Corpus ID: 109375613.

[37] Kurt D. S., James E. B., Monty J. W., Karim C., Julie M. V., Thomas Y., (2017). Using Falling Weight Deflectometer Data with Mechanistic-Empirical Design and Analysis, Volume I: Final Report, FHWA-HRT-16-009.

[38] Kassem E., Muftah A., (2023). Simplified Analysis Methods of TSD and FWD Data for Effective Asphalt Pavement Preservation Program, Idaho Transportation Department, Report No: FHWA-ID-23-294.

[39] Surface layer. WishesCards. 05.07.2025 tarihinde alındı. https://wishescards.ru/surface/layer/

[40] Saltan M., Karaşahin M., (2001). Sonlu Elemanlar Yöntemiyle Esnek Üstyapılarda Tabaka Özelliklerinin Geri Hesaplanması, İMO. Teknik Dergi, 2379-2400, Yazı 163.

[41] Federal Highway Administration, (2017). Using Falling Weight Deflectometer Data with Mechanistic-Empirical Design and Analysis, Volume III: Guidelines for Deflection Testing, Analysis, and Interpretation, Chapter 3. General Backcalculation Guidelines, Federal Highway Administration Research and Technology Coordinating, Developing, and Delivering Highway Transportation Innovations, FHWA-HRT-16-011.

[42] Gupta V. K., Hodouin D., Berube M. A., Everell M. D., (1981). The Estimation of Rate and Breakage Distribution Parameters From Batch Grinding Data For A Complex Pyritic Ore Using A Back-Calculation Method, Powder Technol, 28:97–106. https://doi.org/10.1016/0032-5910(81)87016-7

Research Article

JOURNAL OF CERAMICS AND COMPOSITES

e-ISSN: 3062-293X

Investigation of Waste Foundry Sand as an Eco-Friendly Fine Aggregate Replacement in Asphalt Concrete

Bekir Aktaş[a,*], Ümüt Bora Karabel[b]

[a]Dep. of Civil Engineering, Engineering Faculty, Erciyes University, Türkiye
[b]Dep. of Civil Engineering, Engineering Faculty, Abdullah Gül Univ., Türkiye

Highlights

- Higher WFS ratios tend to reduce Marshall stability and MQ values
- The addition of WFS improves flow levels and VFA
- WFS offers environmental benefits, its incorporation needs careful consideration to maintain asphalt durability.

Abstract

This study investigates the use of Waste Foundry Sand (WFS), a byproduct of the metal casting industry, as a partial replacement for fine mineral aggregates in asphalt concrete production. WFS is often discarded as waste, contributing to environmental concerns in landfills. However, its composition and gradation make it a promising alternative material for road construction, offering both cost and ecological benefits. It is noteworthy that Türkiye is an important metal casting producer in Europe and the world, yet there aren't many studies on this topic. The predominant domain of waste material utilization is the road sector, and the objective of this study was to examine the potential benefits and constraints of integrating WFS into asphalt mixtures. In this study, several asphalt mixes were prepared with varying percentages of WFS sourced from foundries in Türkiye, and tested using the Marshall Mix Design method. In levels not previously explored in the literature, 5 different WFS replacement ratios (0%, 3%, 6%, 9% and 12%) and 6 different bitumen contents (ranging between 3.5% to 6%) were tested, resulting in a total of 36 different mix ratios. The results indicated that as WFS content increased, the flow and elasticity values increased, while a reduction in Marshall stability and Marshall Quotient (MQ) values was observed. Mixes with 9% WFS content exhibited the best performance in terms of flow, while high WFS contents negatively impacted stability and MQ values. These findings suggest that WFS could be a viable material for asphalt concrete; however, careful optimization is necessary to balance performance, cost, and environmental impact. Furthermore, the variability of WFS quality and its long-term performance effects warrant further investigation.

Information

Received:
19.01.2025
Received in revised:
10.03.2025
Accepted:
17.03.2025

Keywords: *Waste foundry sand, Fine aggregate replacement, Asphalt concrete, Environmental sustainability*

1. Introduction

Asphalt concrete, composed of approximately 90% mineral aggregates by weight, relies on the properties of these aggregates to determine the performance and durability of flexible pavements under traffic and climatic stresses [1]. While modified asphalt improves performance, it also increases costs. On the other hand, using waste materials offers a cost-effective and environmentally friendly alternative [2]. The growing accumulation of waste has raised concerns about environmental conservation, driving the exploration of new recycling methods, particularly for industrial and urban solid waste [3]. Highway engineering, with its substantial demand for raw materials, holds significant potential for such practices [4].

According to global casting production statistics, Türkiye is the third-largest metal casting producer in Europe and the eleventh-largest worldwide. Türkiye's Ministry of Environment and Urbanization's Guide Document for the casting sector states that for every ton of metal casting produced, 0.2-0.5 tons of casting waste is generated, with 65% of this waste originating from WFS [5]. Due to the metals absorbed during the casting process and associated environmental concerns, WFS is often

*Corresponding author: baktas@erciyes.edu.tr (Bekir Aktaş), +90 352 207 6666

considered waste and disposed of in landfills. However, WFS possesses suitable engineering properties, making it reusable in the field of civil engineering

WFS typically lack plasticity, with a material percentage smaller than 0.075 mm ranging from 5-12%. Their grain size distribution is uniform, and their shape is generally round to semi-angular. Due to their similarities to natural sand, WFS can effectively replace aggregates in various construction and geotechnical applications. These include its use as fine aggregates in asphalt concrete, hot mix asphalt, road construction, fills, retaining structures, hydraulic barriers, cover layers, backfills, pipe bedding, and in the production of construction materials such as cement, concrete, flowing fills, bricks, blocks, and paving stones [6].

Currently, approximately 60 million tons of WFS are produced globally each year, leading to significant environmental issues due to improper disposal and limited landfill space. Although classified as non-hazardous, WFS's chemical composition poses potential environmental risks. Studies have shown that incorporating WFS into hot mix asphalt (HMA) reduces these environmental threats, as the asphalt binder encapsulates harmful substances, ensuring compliance with major environmental standards [7].

Dyer et al. (2018) investigated the use of WFS as a replacement for fine aggregate in hot mix asphalt (HMA), with substitution rates of 50% and 100% by weight [8]. Physical, mechanical, and microscopic analyses demonstrated that WFS-containing HMA met AASHTO standards, with the asphalt matrix encapsulating hazardous substances and mitigating environmental risks. While WFS mixtures required higher asphalt binder content compared to control mixtures, they exhibited similar mechanical properties, highlighting both their technical viability and environmental sustainability for asphalt pavement applications.

Shuaibu et al. (2019) explored the use of WFS as a partial replacement for cement as filler in asphalt concrete, with substitution levels up to 60% [9]. Using the Marshall design method, they determined an optimum bitumen content (OBC) of 5.5%, and the mix with 60% WFS demonstrated satisfactory strength and durability properties, meeting Nigerian General Specification for Roads and Bridges (NGSRB) requirements for flexible pavement wearing courses. The study highlighted the potential of WFS to conserve primary materials, reduce landfill waste, and provide a cost-effective, sustainable alternative filler for asphalt concrete.

Dyer et al. (2020) investigated the use of WFS as a substitute for manufactured sand in hot mix asphalt (HMA) at replacement rates of 25%, 50%, 75%, and 100%, using materials from industrial landfills and active foundries [10]. Their findings showed that the mechanical performance of WFS-containing HMA, assessed through splitting tensile strength and resilient modulus tests, was comparable to conventional mixtures up to certain replacement levels. While the study demonstrated the technical and environmental feasibility of using WFS in asphalt pavements, it did not explore low replacement percentages (3–12%) and lacked data on stability, flow, and Marshall Quotient (MQ) across varying bitumen contents and WFS ratios.

After a comprehensive review, Dyer and Lima (2022) emphasized that using WFS as an aggregate in HMA represents an area for continued research, as real-world applications are needed to contribute to a circular economy in the construction industry and mitigate the effects of its accelerated growth [11].

Gambalonga et al. (2023) evaluated the incorporation of WFS, obtained from automotive parts manufacturing, into asphalt mixtures, focusing on three WFS types: molding sand (MS), fine dust (FDE), and a laboratory-prepared blend (BL, 80% MS and 20% FDE) [12]. Using the Marshall method, they found that mixtures with 10% BL and 5% asphalt binder content achieved optimal mechanical properties (e.g., stability of 658 kgf, 3.3% air void volume) while meeting technical and environmental standards. Their study highlighted the feasibility of using WFS in asphalt mixtures but emphasized that results depend on the WFS generation process and project-specific requirements. Although not explicitly highlighted in the conclusions, the presented graphs indicate that samples without WFS exhibit significantly higher Marshall stability values across various bitumen contents compared to those containing WFS.

WFS is a byproduct of the metal casting industry, and its potential for reuse has gained increasing recognition in recent years. Typically, WFS is generated when foundry sands, after multiple cycles of use, can no longer be effectively recycled in casting processes. Historically, WFS has been disposed of in landfills, contributing to environmental pollution. However, due to its composition and granulation, WFS is becoming an attractive option for reuse, particularly in road construction, soil stabilization, and other civil engineering applications. Reusing WFS not only mitigates environmental impacts but also reduces reliance on natural resources, thus providing both economic and ecological benefits.

The primary objective of this research was to assess the performance characteristics of asphalt mixtures incorporating Waste Foundry Slag (WFS) by evaluating key material properties and conducting various laboratory tests. As documented in the literature and emphasized by previous studies, a significant gap exists in research regarding the mechanical properties of Hot Mix Asphalt (HMA) containing WFS [7]. Moreover, there is a notable scarcity of studies on this subject within Türkiye, despite the country ranking as the third-largest metal

casting producer in Europe and the eleventh-largest globally. Given the widespread use of bitumen in Türkiye's metal production sector, this study sought to explore the potential advantages and limitations of incorporating WFS into asphalt mixtures. To achieve this, various samples were fabricated using different bitumen contents and replacement levels, some of which have not been explored in the existing body of literature. Preliminary assessments were carried out through well-established Marshall design tests, thereby contributing valuable insights into the feasibility of using WFS in asphalt concrete.

2. Materials

2.1. Waste Foundry Sand (WFS)

In this study, WFS from the process of a casting company serving the vehicle, machinery, and equipment manufacturing sectors in Bursa and Manisa, Türkiye, was utilized. The collected material was sieved through granulometric screens, and the passing No. 4 sieve was incorporated into mixtures at varying proportions.

Table 1. Gradation of the WFS

Sieve Designation	3/8"	#4	#10	#40	#80	#200
Nominal Sieve Opening (mm)	9.51	4.76	2.00	0.420	0.177	0.074
Percentage Passing, %	99,9	99,5	99,5	95,1	44,0	11,4

2.2. Mineral Aggregates

A specific type of limestone was utilized as coarse and fine aggregate in asphalt concrete production. The crushed aggregate was sourced from the Bürüngüz quarry located in Kayseri, Türkiye. The materials were classified into fractions of 0/5, 5/12.5, and 12.5/19.5 mm. Table 2 presents the physical and mechanical properties of the limestone aggregate used in this study, along with the corresponding requirements for binder course specifications as per the relevant TS EN standards.

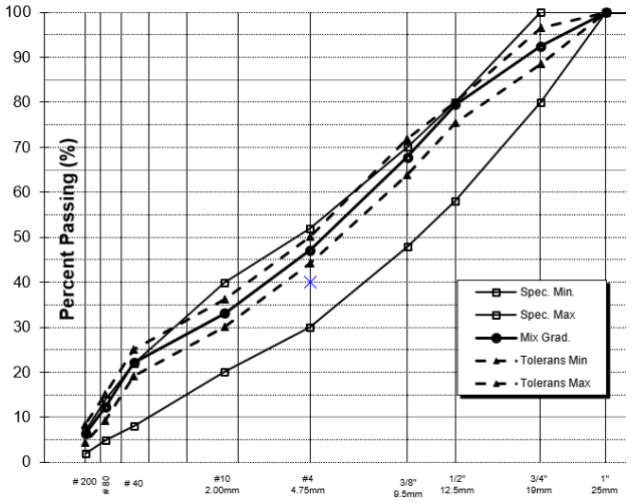

Figure 1. Granulometry curve of the used aggregates

Table 2. Characteristics of the limestone aggregate

Test	**Requirements for binder cource**	**Filler**	**Fine Agg.**	**Coarse Agg.**
Flakiness Index (%)	< 35	-		8.4
Bulk Specific Gravity (gr/cm^3)	-	2.738	2.616	2.662
LA Fragmentation (%)	< 25	-	-	19.76
Nicholson Stripping (%)	> 50	-	-	70-80
Freeze-Thaw Resistance (%)	< 12	-	-	0.12

3. Experimental Programmes

To assess the feasibility of utilizing WFS in the binder course of asphalt concrete, WFS passing through a 4.75 mm sieve (#4) was used as a partial replacement for mineral aggregates of the same size. The replacement ratios were adjusted based on varying percentages of WFS. For each mixture containing WFS, the Marshall Mix design method was employed to produce asphalt concrete. Subsequently, Marshall Stability and flow tests were conducted to evaluate the mechanical properties of the mixtures. Asphalt mixtures were prepared with varying WFS content at 3.0%, 6.0%, 9.0%, and 12.0% by weight of the dry mix. The limestone aggregate ratios and WFS ratios (%) are provided in Table 3.

Table 3. Specimen code of asphalt concrete for each mix design

Specimen Codes	Limestone Aggregate Ratios (%)	WFS Ratios (%)
M1	100	0
M2	97	3
M3	94	6
M4	91	9
M5	88	12

3.1. Mix Design

Limestone and WFS aggregates, along with 50/70 penetration grade asphalt, were used to fabricate the asphalt concrete specimens. The bitumen utilized in this study was pure 50-70 penetration grade, produced by the TUPRAS Company in Türkiye. The characteristics of the bitumen were verified in accordance with ASTM standards. The bitumen had a penetration grade of 57, and its bulk specific gravity was 1.027. The aggregate gradation for all mixtures was selected based on the guidelines set by the Turkish General Directorate of Highways (KGM). For the standard Marshall specimens, the total weight of the aggregate was adjusted to 1150 g. Additionally, seventy-five blows were applied to compact the specimens, ensuring the appropriate density for testing.

3.2. Marshall Stability Test

The asphalt mixtures were designed using the standard Marshall Mix design procedure. Specimens were 10.16 cm in diameter and 6.35 cm thick. Tests included bulk specific gravity, performance (stability and flow), and maximum theoretical specific gravity. Specimens were prepared with bitumen ratios of 3.5%, 4.0%, 4.5%, 5.0%, 5.5%, and 6.0%.

4. Results And Discussion

The results are presented in Figures 2–8. Figure 2 depicts the bulk specific gravity values of compacted hot mix asphalt (G_{mb}) in g/cm³ on the vertical axis for specimens with varying WFS ratios, plotted against bitumen content percentages on the horizontal axis. G_{mb} plays a crucial role in determining the volumetric properties of the mixtures, including Voids in Total Mix (VTM), Voids in Mineral Aggregate (VMA), and Voids Filled with Bitumen (VFB) or Filled with Asphalt (VFA) [13]. However, preliminary evaluations can also be made using these G_{mb} values. The results indicate that G_{mb} values increased with bitumen content up to 5.5%, after which they plateaued, showing no significant further increase at higher bitumen contents. Notably, specimens with 0% WFS consistently exhibited the lowest G_{mb} values across nearly all bitumen content levels. While the highest G_{mb} values were occasionally observed at 12% WFS for certain bitumen contents, in most cases, the maximum G_{mb} values occurred at 9% WFS. Beyond this range, both higher and lower WFS ratios led to a reduction in G_{mb} values. However, some preliminary evaluation can be made using these G_{mb} values. As observed, the G_{mb} values increased with bitumen content up to 5.5%, where they reached a plateau, and no further increase was recorded with higher bitumen contents. Notably, the lowest G_{mb} values were consistently observed in specimens with 0% WFS across nearly all bitumen content levels. Furthermore, while the highest G_{mb} values were achieved at 12% WFS for a few bitumen contents, most cases exhibited maximum G_{mb} values at 9% WFS. Beyond this range, both higher and lower WFS ratios resulted in reduced G_{mb} values.

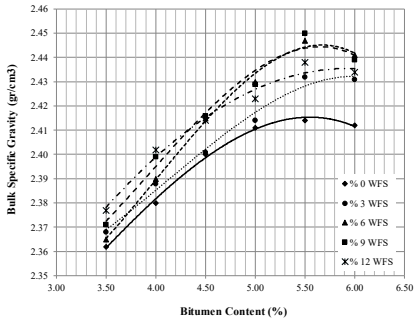

Figure 2. Variation of bulk specific gravity (G_{mb}) values (g/cm³) with bitumen content for specimens containing different WFS ratios

Figure 3 shows the relationship between bitumen content (%) on the horizontal axis and VFA (%) on the vertical axis for specimens with varying WFS ratios. VFA indicates the percentage of VMA filled with asphalt binder instead of air voids. Maintaining sufficient air voids prevents bleeding by allowing asphalt to compress without forcing binder out from between the aggregate particles. If VFA is too high, the binder has no space to move during pavement compression, causing potential issues. According to Asphalt Institute criteria, the VFA should be between 65% and 80%, depending on traffic load. For heavy traffic, it is recommended to maintain VFA values within the 65–75% range. As seen in Figure 3, VFA values increase proportionally with bitumen content. Specimens with 0% WFS consistently exhibit the lowest VFA values, while those with 9% WFS achieve the highest.

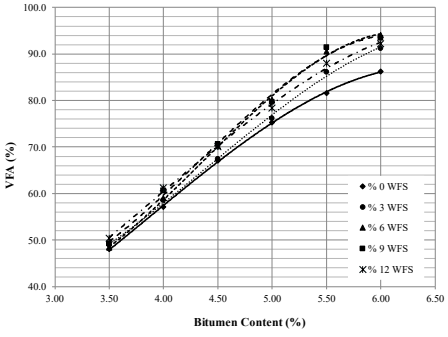

Figure 3. Variation of voids filled with asphalt (VFA, %) with bitumen content (%) for mixtures containing different WFS ratios

Figure 4 illustrates the relationship between bitumen content (%) on the horizontal axis and VMA (%) on the vertical axis for specimens with varying WFS ratios. The VMA values initially decrease with increasing bitumen content, stabilizing around 4.5–5.5%, and then begin to increase with further increases in bitumen content. Among the WFS ratios, 0% WFS consistently exhibits the highest VMA values across all bitumen content levels, while the bitumen content corresponding to the minimum VMA varies based on the WFS ratio. The reduction in VMA values can be attributed to the finer particle sizes and smoother, more spherical surface texture of WFS compared to crushed limestone sand. Crushed limestone sand, being more angular, has a higher void content, which contributes to a higher VMA. In contrast, the smoother, rounded characteristics of WFS particles reduce the void content, leading to a decrease in VMA.

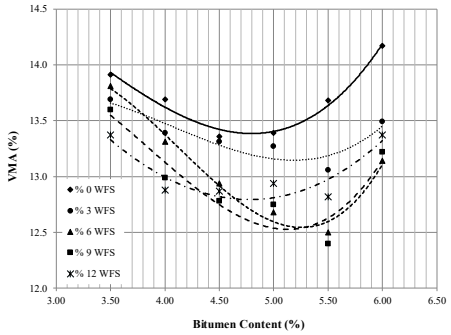

Figure 4. Variation of voids in mineral aggregates (VMA, %) with bitumen content (%) for mixtures containing different WFS ratios

Figure 5 illustrates the flow levels (mm) for varying bitumen contents (%) at each WFS ratio. The results show that flow levels increase with rising bitumen content across all WFS ratios. The highest flow values are observed for 12% WFS, followed by 9% WFS, while the lowest flow levels are consistently recorded at 0% WFS for all bitumen contents. These results align with previous findings. The increase in flow values can be attributed to the smoother, more spherical surface texture of WFS compared to crushed limestone sand. Crushed limestone sand, being more angular, restricts flow, contributing to a lower flow value. In contrast, the smoother, rounded characteristics of WFS particles enhance the flow. The flow value needs to be maintained within an optimal range, as higher flow values lead to plastic behavior in the mixture, while lower flow values may result in durability issues [14]. It is observed that, while the flow increases with bitumen content in the control sample with 0% WFS, the flow level achieved at 6% bitumen content in the control specimen is easily reached at just 3.5% bitumen content in specimens with 9-12% WFS. Therefore, it is evident that the incorporation of WFS enhances the flow values of the specimens. Consequently, it is imperative to exercise caution with regard to potential durability concerns and long-term loading conditions.

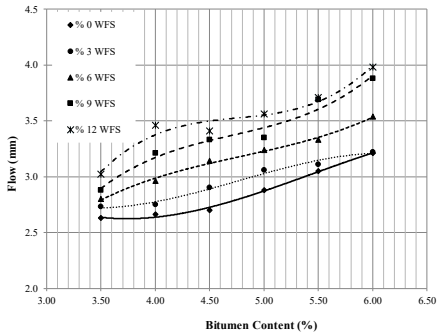

Figure 5. Flow levels (mm) as a function of bitumen content (%) for mixtures with varying WFS ratios

Figure 6 presents the Marshall stability measurements (kN) for various bitumen contents (%) and WFS ratios. The results indicate that stability values increase with bitumen content up to a certain point, after which they plateau and then decrease. The highest stability values are observed within the bitumen content range of 4.35% to 5%. Notably, the highest stability values across all bitumen contents are achieved with 0% WFS, followed by 3% WFS and 6% WFS. It is also evident that as the WFS ratio increases, the stability values generally decrease. These findings are consistent with previous results. The reduction in stability values can be attributed to the smoother, more spherical surface texture of WFS compared to crushed limestone sand. Crushed limestone sand, being more angular, enhances stability, contributing to a higher stability value. In contrast, the smoother, rounded characteristics of WFS particles decrease stability, leading to lower stability values. However, a stability value of 8 kN is typically sufficient for most road designs, including those under heavy load conditions [11]. On the other hand, it is important to note that Marshall stability may not always correlate with the long-term stability of an asphalt mixture in pavement performance. Therefore, although WFS usage results in a significant reduction in stability values, it is still possible to develop a design that satisfies the minimum project requirements by considering other important benefits provided by WFS. Nonetheless, it is crucial to ensure that project stability requirements are met, and attention should be given to potential performance reductions under long-term loading conditions.

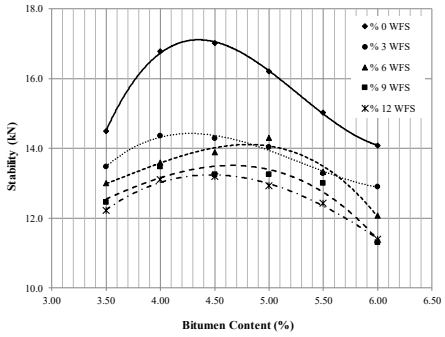

Figure 6. Marshall stability (kN) values for mixtures with varying bitumen contents (%) and WFS ratios

Figure 7 presents the Marshall Quotient (MQ) measurements (kN/mm) for varying bitumen contents (%) and WFS ratios. The data shows that MQ values generally decrease as bitumen content increases. The highest MQ values are observed at 0% WFS, followed by 3% WFS and 6% WFS. Additionally, it is clear that MQ values tend to decrease as the WFS ratio increases. These findings are consistent with previous observations, where increasing WFS content leads to a decrease in stability, while flow values rise. Since the Marshall Quotient is the ratio of stability to flow, WFS usage further reduces the quotient (due to both a decrease in the numerator and an increase in the denominator). Literature suggests that the Marshall Quotient provides valuable insight into the stiffness modulus of the mixture and serves as an important indicator for predicting fatigue life (i.e., the higher the stiffness, the longer the fatigue life) [15]. Therefore, although WFS usage significantly enhances flow values, designers must ensure that project stability and MQ requirements are met, especially under long-term or high-cycle loading conditions.

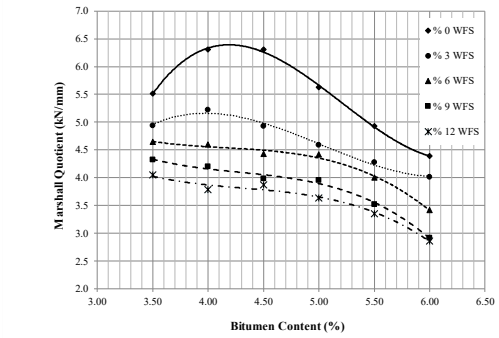

Figure 7. Marshall Quotient (MQ) values (kN/mm) for various bitumen contents (%) and WFS ratios

5. Conclusion and Recommendation

In this study, the potential of WFS in asphalt concrete production was investigated. WFS was sourced from casting companies in Bursa and Manisa, Türkiye, and sieved to isolate material passing No.4 sieve. This material was then incorporated into asphalt mixtures at varying proportions. The Marshall Mix Design method was applied to prepare the asphalt mixtures, and the impact of bitumen content on the performance of WFS-modified asphalt mixtures was evaluated through Marshall Design tests. The bulk specific gravity, voids filled with asphalt, and Marshall stability values were all affected by the proportion of WFS, with certain mixtures exhibiting improved characteristics at specific WFS content levels. Based on the results, the study makes the following key observations:

-Bulk specific gravity (G_{mb}) values increased with bitumen content up to 5.5%, plateaued thereafter, with the lowest values observed at 0% WFS. The highest G_{mb} values were generally achieved at 9% WFS.

-Voids filled with asphalt (VFA) values increased proportionally with bitumen content, with 9% WFS consistently yielding the highest VFA values, while 0% WFS produced the lowest values. Conversely, voids in mineral aggregates (VMA) values initially decreased with rising bitumen content but stabilized around 4.5%-5.5%. The highest VMA values were consistently observed at 0% WFS, which is essential for predicting the durability and performance of hot-mix asphalt pavement.

-Flow levels increased with rising bitumen content across all WFS ratios, with the highest flow values observed at 12% WFS and the lowest at 0% WFS. Since flow indicates the plasticity and flexibility of the asphalt mixture, the results emphasize the importance of achieving an optimal asphalt content to ensure durability and performance under traffic.

-Marshall stability values increased with bitumen content up to a certain level, with the highest stability observed at 0% WFS, followed by 3% and 6% WFS. The results indicate that higher WFS ratios tend to reduce stability, which is crucial for predicting pavement performance under traffic loads and weather conditions, where higher stability values are needed for better resistance to rutting and deformation.

-Marshall Quotient (MQ) values decreased with increasing bitumen content, with the highest values observed at 0% WFS, followed by 3% and 6% WFS. These results suggest that higher WFS ratios lead to lower MQ values, indicating reduced resistance to shear stresses and permanent deformation, which could affect the material's performance in resisting rutting.

Based on these findings, the use of WFS generally has a negative impact on key properties such as stability and resistance to shear stresses, as higher WFS ratios tend to reduce stability and Marshall Quotient (MQ) values. However, WFS can enhance certain properties such as flow levels, suggesting its potential benefits in terms of flexibility and optimization of asphalt binder content, though its overall effect on durability requires careful consideration. While WFS offers significant advantages, including cost-effectiveness, environmental benefits, and a reduction in landfill waste, there are critical challenges to address. The incorporation of WFS in construction materials requires a careful balance, as excessive use can negatively affect material properties like stability and flow. Additionally, the variability in WFS quality across different foundries may pose challenges in ensuring consistent material performance. Therefore, further research is essential to optimize the use of WFS in asphalt concrete.

Declaration of Interest Statement

The authors declare that they have no known competing financial interests or personal relationships that could

have appeared to influence the work reported in this paper.

References

[1] Brown, E. R., Kandhal, P. S., Roberts, F. L., Kim, Y. R., Lee, D.-Y., & Kennedy, T. W. (2009). Hot mix asphalt materials, mixture design, and construction. Lanham: NAPA Research and Education Foundation.

[2] Arabani, M., Mirabdolazimi, S. M., & Sasani, A. R. (2010). The effect of waste tire thread mesh on the dynamic behaviour of asphalt mixtures. Construction and Building Materials, 24(6), 1060–1068. https://doi.org/10.1016/j.conbuildmat.2009.12.016

[3] Republic of Türkiye, Ministry of Environment and Forestry General Directory of Environmental Management. (2008). Waste management action plan (2008–2012). Ankara.

[4] Pérez, I., Pasandín, A. R., & Medina, L. (2012). Hot mix asphalt using C&D waste as coarse aggregates. Materials & Design, 36, 840–846. https://doi.org/10.1016/j.matdes.2011.11.012

[5] Eren, Ş. (2020). A resource survey on the use of waste foundry sand by substituting natural aggregate in industrial waste-based geopolymer concrete. Gazi Üniversitesi Fen Bilimleri Dergisi Part C: Tasarım ve Teknoloji, 8(3), 746–757. https://doi.org/10.29109/gujsc.712111

[6] Balkaya, M. (2022). Atık döküm kumunun geoteknik mühendisliği uygulamalarında kullanımı. Ulusal Çevre Bilimleri Araştırma Dergisi, 5(2), 92–99.

[7] Dyer, P. P. O. L., Klinsky, L. M. G., Silva, S. A., & de Lima, M. G. (2020). Mechanical and structural assessment of hot mix bituminous mixtures containing waste foundry sand. International Journal of Pavement Engineering, 22(14), 1801–1812. https://doi.org/10.1080/10298436.2020.1724290

[8] Dyer, P. P. O. L., Coppio, G. J. L., Silva, S. A., Cividanes, L. S., Klinsky, L. M. G., & de Lima, M. G. (2021). Mechanical and microstructural assessments of waste foundry sand in hot mix asphalt. Construction and Building Materials, 311, 125329. https://doi.org/10.1016/j.conbuildmat.2021.125329

[9] Shuaibu, A. A., Otuoze, H. S., Mohammed, A., & Lateef, M. A. (2019). Properties of asphalt concrete containing waste foundry sand (WFS) as filler material. Arid Zone Journal of Engineering, Technology and Environment, 15(3), 662–677.

[10] Dyer, P. P. O. L., Klinsky, L. M. G., Silva, S. A., & de Lima, M. G. (2020). Mechanical and structural assessment of hot mix bituminous mixtures containing waste foundry sand. International Journal of Pavement Engineering, 22(14), 1801–1812. https://doi.org/10.1080/10298436.2020.1724290

[11] Dyer, P. P. O. L., & de Lima, M. G. (2022). Waste foundry sand in hot mix asphalt: A review. Construction and Building Materials, 359, 129342. https://doi.org/10.1016/j.conbuildmat.2022.129342

[12] Gambalonga, B., Nicolini, J. L., Inocente, J. M., Pich, C. T., Angioletto, E., Pereira, F. R., Montedo, O. R. K., & Arcaro, S. (2023). Valorization of waste foundry sand aggregates in hot-mix asphalt. Process Safety and Environmental Protection, 173, 277–288. https://doi.org/10.1016/j.psep.2023.03.025

[13] Gardete, D., Picado-Santos, L., Capitão, S., & Luzia, R. (2022). Asphalt mix design: Discussion on the bulk specific gravity procedure influence on the results obtained from empirical, volumetric, and performance-based methods. Construction and Building Materials, 342, 127870. https://doi.org/10.1016/j.conbuildmat.2022.127870

[14] Yaacob, H., Chang, F. L., & Hainin, M. R. (2014). Marshall properties of single-face-compacted asphalt specimen. Materials Research Innovations, 18(2), 121–125. https://doi.org/10.1179/1432891714Z.000000000942

[15] Tapkın, S. (2008). Mechanical evaluation of asphalt–aggregate mixtures prepared with fly ash as a filler replacement. Canadian Journal of Civil Engineering, 35(1), 27–40. https://doi.org/10.1139/L07-082

Research Article

JOURNAL OF CERAMICS AND COMPOSITES

e-ISSN: 3062-293X

Effect of elevation on wood density of oriental beech (*Fagus orientalis* lipsky): A case study from Daday

Emre KUZUGÜDENLİ[a,*]

[a] *Department of Forestry, Yenisarbademli Vocational School, Applied Sciences University of Isparta, Isparta, Turkey*

Highlights

- Elevation has a strong negative effect on oven-dry wood density in Fagus orientalis
- Mean wood density decreased by 13% from low to high elevation zones
- The relationship between elevation and wood density showed a very strong correlation (r = –0.84)
- Low-elevation stands are more suitable for producing high-quality beech timber

Abstract

This study examines the relationship between oven-dry wood density and the site factor of elevation in Oriental beech (*Fagus orientalis* Lipsky). The research was conducted in three natural stands located at different elevation zones (low: 250–500 m, mid: 800–1100 m, high: 1400–1700 m) within the Daday Forest District of Kastamonu province in Turkey. From each elevation group, wood samples were collected from 10 trees and analyzed according to the TS 2472 standard for oven-dry density. The data were evaluated using ANOVA and Pearson correlation analysis. Results revealed a strong negative correlation between elevation and wood density ($r = –0.84$; $p < 0.001$). The mean oven-dry density was 0.712 g/cm³ at low elevation, decreasing to 0.617 g/cm³ at high elevation. These findings demonstrate that wood quality depends not only on species but also on site conditions, offering valuable insights for silvicultural planning and industrial wood production.

Information

Received:

11.05.2025

Received in revised:

27.05.2025

Accepted:

14.06.2025

Keywords: Wood density, elevation, oriental beech

1. Introduction

Wood is a key renewable raw material that plays a central role not only in the forestry sector but also in construction, furniture, paper, and bioenergy industries. Among the most critical physical properties influencing the industrial value and performance of wood is wood density, defined as the dry mass per unit volume. This property is directly linked to structural integrity, processing behavior, and durability of wood products. High-density woods are typically more durable and mechanically resistant but are harder to process, whereas low-density woods are lighter and easier to work with but may lack strength and decay resistance [1].

Wood density is influenced by both genetic characteristics and site conditions. Environmental factors that shape wood formation are commonly categorized into four major categories: physiographic, climatic, edaphic, and biotic [2]. Among these, elevation (i.e., altitude above sea level) is a major physiographic factor with the capacity to affect wood structure directly and indirectly. Increasing elevation often brings a decrease in mean annual temperature, shorter growing seasons, changes in radiation, and variations in soil development and moisture availability. These environmental shifts affect photosynthesis, cambial activity, and xylem differentiation, ultimately modifying wood anatomy and density [3].

Numerous studies have reported that elevation can significantly affect wood density. In particular, many species show a negative correlation between elevation and wood density, attributed to cooler temperatures and limited cambial activity at higher altitudes [4]. Chave et al. [5], in a comprehensive study of 2,456 tropical tree

* *Corresponding author: emrekuzugudenli@isparta.edu.tr (E., Kuzugüdenli), +90 536 783 2444*

species, found that wood density declined with elevation, suggesting that reduced lignification and lower vessel wall thickness were responsible. Similarly, Govorčin et al. [6] reported that beech trees in Croatia showed decreasing mechanical and density properties with increasing elevation.

On the other hand, not all studies agree on this trend. Kiaei [7], investigating *Carpinus betulus* L. in northern Iran, observed a positive correlation between elevation and wood density. This anomaly was explained by differences in tree age—higher elevation stands comprised younger trees with higher juvenile wood content. Such discrepancies highlight the importance of controlling for variables like tree age, soil type, and competition when analyzing site–wood property relationships [8].

In Turkey, Oriental beech (*Fagus orientalis* Lipsky) is one of the most ecologically and economically important native tree species, with a wide natural distribution in the Black Sea region. Its high-quality wood is widely used in furniture and veneer industries, and the species is considered highly responsive to ecological gradients, making it a suitable model for studying site–trait interactions [9]. Previous research on *F. orientalis* indicates that elevation affects multiple wood properties, including fiber length, ring width, vessel diameter, and ultimately, density [10].

Elevation also impacts the structure of annual growth rings. Trees growing at higher elevations generally experience shortened growing seasons and reduced cambial activity, resulting in narrower rings and less lignified latewood. These changes can lead to lower overall wood density [11]. However, species-specific traits, microsite effects, and stand structure can moderate or obscure these elevation-induced patterns, underlining the need for species- and site-specific investigations [12].

This study aims to investigate the relationship between elevation and a single wood property, oven-dry wood density, in oriental beech under natural forest conditions in Turkey. By isolating a single site factor and a single wood trait, the study avoids the complexity of multivariate ecological analyses and instead provides a focused and interpretable assessment of how altitude affects wood structure. The results are expected to contribute to more informed silvicultural planning and sustainable forest management, particularly in site selection and stand design for high-quality wood production.

2. Materials and Methods

2.1. Study area

The study was carried out in the Daday Forest Enterprise Directorate, located in Kastamonu Province, situated within the Western Black Sea Region of Turkey. This region exhibits a wide altitudinal gradient, ranging from 250 meters to approximately 1700 meters above sea level, making it well-suited for evaluating the effects of elevation on tree growth characteristics within a relatively homogeneous climate zone. The area is topographically diverse, with undulating mountainous terrain and a predominance of north- and east-facing slopes.

The region is classified as a transition zone between the Black Sea maritime climate and the semi-continental interior climate. It receives annual precipitation of approximately 900–1100 mm and has mean annual temperatures ranging between 9°C and 11°C [13]. The forests in the region are dominated by Oriental beech, along with Scots pine (*Pinus sylvestris*), fir (*Abies nordmanniana* subsp. *bornmuelleriana*), and several species of oak (*Quercus* spp.). These conditions provide a stable ecological framework for the analysis of site–wood property interactions [14].

2.2. Sampling design

To examine the relationship between elevation and oven-dry wood density, three distinct elevation bands were defined:

- Low elevation: 250–500 m
- Mid elevation: 800–1100 m
- High elevation: 1400–1700 m.

In each elevation band, 10 mature Oriental beech trees were selected, totaling 30 sample trees. Trees were selected based on their dominance in the canopy, absence of visible defects, and similar stem forms. Stands were chosen with comparable site characteristics (e.g., slope, aspect, soil type) and management history to minimize confounding environmental variation. The trees ranged in age from 80 to 120 years, which helped minimize potential age-related variation in wood properties [15].

2.3. Wood sampling and density determination

From each sample tree, a 5-cm-thick cross-sectional disc was removed at breast height (1.30 m). Discs were labelled and transported to the laboratory. In the lab, the samples were first air-dried, then oven-dried at 103 ± 2°C until reaching constant weight.

Each disc was subdivided radially into three 2 × 2 × 3 cm prisms representing different positions between the pith and bark. For each prism, volume was measured using the water displacement method, and oven-dry mass was determined with an analytical balance (±0.001 g precision) (see Figure 1.).

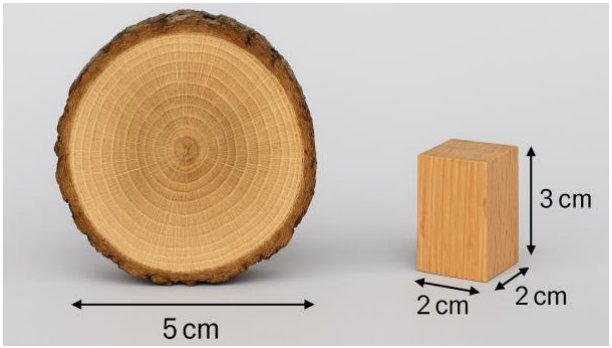

Figure 1. Wood sampling procedure: Cross-Sectional disc (left) and prism used for density analysis (right)

2.4. Statistical analyses

All data were evaluated for normality using the Shapiro-Wilk test, and results indicated normal distribution in all groups. Thus, parametric statistical methods were used. Differences in mean oven-dry density among the elevation groups were analysed using one-way ANOVA. Where significant differences were found, Tukey's HSD test was applied for post-hoc comparisons [16].

The strength and direction of the relationship between elevation and wood density were assessed using Pearson correlation analysis. Correlation coefficients were interpreted based on Evans (1996), as follows:

- 0.00–0.19: Very weak
- 0.20–0.39: Weak
- 0.40–0.59: Moderate
- 0.60–0.79: Strong
- 0.80–1.00: Very strong [17].

All statistical analyses were performed using SPSS v25.0, and significance was tested at $p < 0.05$.

2.5. Limitations

This study deliberately focused on a single wood trait (oven-dry density) and one environmental factor (elevation) to isolate their relationship. While other variables such as soil chemistry, competition, or light availability may influence wood formation; however, their effects were minimized by carefully selecting homogeneous stand conditions. Nonetheless, future studies may expand upon these results by incorporating additional structural or anatomical traits such as vessel diameter, ring width, or fiber length using micro-sectioning and image analysis techniques [18].

3. Results

Statistical analysis revealed that oven-dry wood density in oriental beech varied significantly across the three elevation classes. The mean density values for each group showed a consistent decreasing trend with increasing elevation, as summarized in Table 1 and Figure 2.

Table 1. Mean oven-dry wood density by elevation class

Elevation Class	Mean Density (g/cm³)	Std. Dev.	Min.	Max.
Low (250–500 m)	0.712	0.017	0.689	0.735
Mid (800–1100 m)	0.664	0.020	0.637	0.689
High (1400–1700 m)	0.617	0.018	0.591	0.639

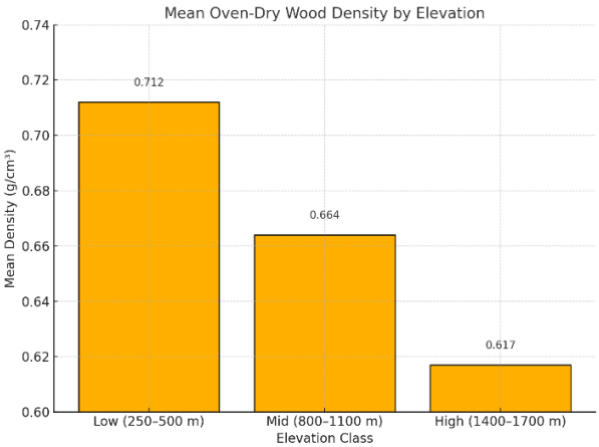

Figure 2. Mean oven-dry wood density by elevation class

The ANOVA test indicated that the differences among the three elevation groups were statistically significant ($F = 58.43$, $p < 0.001$). According to the Tukey HSD test, all pairwise group comparisons were also significant:

- Low vs. Mid: $p = 0.001$
- Low vs. High: $p < 0.001$
- Mid vs. High: $p = 0.002$.

These results suggest that even modest differences in elevation (300–400 meters) can lead to substantial changes in wood density in Oriental beech.

3.1. Correlation between elevation and wood density

To further clarify the relationship, Pearson correlation analysis was conducted between elevation (as a continuous variable) and wood density values. The result showed a very strong and negative correlation ($r = –0.84$, $p < 0.001$). This finding confirms that as elevation increases, oven-dry wood density in oriental beech

decreases significantly. This is consistent with physiological expectations: at higher elevations, lower temperatures and shorter growing seasons can reduce cell wall thickening, thereby lowering wood density [4-6].

3.2. Qualitative field observations

Although the study primarily focused on density values, qualitative anatomical differences were also noted during visual inspection of the cross-sectional discs. Trees from higher elevations generally exhibited:

- Narrower growth rings
- Less distinct earlywood–latewood boundaries
- Lower vessel density and less compact fiber zones.

These features are congruent with anatomical responses reported in previous research on beech and similar temperate broadleaf species growing under suboptimal conditions [10,11].

4. Discussion and Conclusion

The findings of this study clearly demonstrate that elevation is a significant environmental factor influencing oven-dry wood density in oriental beech. The results indicate a consistent and statistically significant decrease in wood density with increasing elevation, with a strong negative correlation ($r = –0.84$, $p < 0.001$). Trees growing at low elevations (250–500 m) produced significantly denser wood than those at mid (800–1100 m) or high elevations (1400–1700 m), a pattern aligned with the known eco-physiological responses of temperate forest species to altitude gradients.

Several mechanisms may explain the reduction in wood density at higher elevations. First, shorter growing seasons and reduced thermal accumulation at higher altitudes limit the duration and intensity of cambial activity, resulting in narrower annual rings and decreased cell wall thickening [4-6]. This phenomenon is particularly important for diffuse-porous hardwoods like beech, where latewood formation contributes substantially to overall density [10]. Furthermore, lower temperatures may alter hormonal balances and resource allocation during xylem development, potentially decreasing lignin and cellulose deposition [19].

These results are consistent with similar studies conducted on both *Fagus sylvatica* [6] and other broadleaved species in mountainous regions [16]. However, discrepancies in the literature—such as Kiaei's [7] report of higher densities at greater altitudes—highlight the complexity of ecological controls on wood structure. Differences in genetic provenance, site productivity, age structure, and stand dynamics may produce species- or region-specific deviations from general patterns [8].

From a silvicultural and industrial perspective, the implications of this study are significant. For forest managers aiming to optimize wood quality in beech stands, low to mid-elevation sites should be prioritized for conservation and timber production purposes. These zones are more likely to produce high-density wood suitable for structural uses, furniture, or veneer manufacturing. In contrast, stands at higher elevations may yield lighter wood more appropriate for pulp or fuelwood purposes. Therefore, elevation data should be integrated into forest management plans, particularly in species–site matching strategies, stand rotation planning, and future yield projections under changing climatic scenarios [13,14].

The results also underscore the value of single-variable ecological studies in isolating specific environmental effects on tree traits. While multivariate models can offer broad predictive power, targeted studies such as this provide clearer insight into cause–effect relationships, especially when carefully controlled for confounding factors such as tree age, stand structure, and soil type [15].

5. Recommendations

Based on the results of this study, the following recommendations are offered:

i. In forest planning, particularly for oriental beech, sites located at lower elevations (below 800 m) should be preferred for high-density wood production.

ii. Future studies should integrate xylem anatomical analysis, dendrochronological methods, and physiological measurements (e.g., lignin/cellulose ratios) to explain the density–elevation relationship at finer resolution.

iii. Incorporating GIS-based modeling with topographic, climatic, and edaphic data layers could help scale this approach to broader landscapes.

iv. Provenance trials and common garden experiments could be used to determine the relative roles of genetics vs. environment in observed wood density variation.

6. Conclusion

In conclusion, elevation plays a significant and measurable role in shaping the oven-dry wood density of oriental beech in natural stands of the Western Black Sea Region of Turkey. The clear decline in density with increasing elevation supports both ecological theory and practical expectations in forestry expectations. This study contributes to the growing body of knowledge on wood

ecology and highlights the importance of integrating environmental gradients into forest productivity and quality assessments.

Declaration of Interest Statement

The authors declare that they have no known competing financial interests or personal relationships that could have appeared to influence the work reported in this paper.

References

[1] Bowyer, J. L., Shmulsky, R., & Haygreen, J. G. (2007). *Forest products and wood science: An introduction* (5th ed.). Blackwell Publishing.

[2] Çepel, N. (1995). *Ekoloji*. İstanbul: İstanbul Üniversitesi Yayınları.

[3] Pretzsch, H., Biber, P., Schütze, G., Uhl, E., & Rötzer, T. (2014). Forest stand growth dynamics in Central Europe have accelerated since 1870. *Nature Communications*, 5, 4967. DOI: 10.1038/ncomms5967

[4] Swenson, N. G., & Enquist, B. J. (2007). Ecological and evolutionary determinants of a key plant functional trait: Wood density and its community-wide variation across latitude and elevation. *American Journal of Botany*, 94(3), 451–459. DOI: 10.3732/ajb.94.3.451

[5] Chave, J., Muller-Landau, H. C., Baker, T. R., Easdale, T. A., Steege, H. T., & Webb, C. O. (2006). Regional and phylogenetic variation of wood density across 2,456 neotropical tree species. *Ecological Applications*, 16(6), 2356–2367. DOI: 10.1890/1051-0761(2006)016[2356:RAPVOW]2.0.CO;2

[6] Govorčin, S., Sinković, T., & Trajković, J. (2003). Some physical and mechanical properties of beech wood grown in Croatia. *Wood Research*, 48(3), 39–52.

[7] Kiaei, M. (2012). Effect of site and elevation on wood density and shrinkage and their relationships in *Carpinus betulus*. *Forestry Studies in China*, 14(3), 229–234. DOI: 10.1007/s11632-012-0307-z

[8] Hacke, U. G., & Sperry, J. S. (2001). Functional and ecological xylem anatomy. *Perspectives in Plant Ecology, Evolution and Systematics*, 4(2), 97–115. DOI: 10.1078/1433-8319-00017

[9] Topaloğlu, H. (2013). Doğu Kayını (*Fagus orientalis Lipsky*)'nda odun anatomik özelliklerinin farklı yükselti basamaklarında değişimi. *Bartın Orman Fakültesi Dergisi*, 15(2), 37–48.

[10] Gierlinger, N., & Schwanninger, M. (2006). Chemical imaging of poplar wood cell walls by confocal Raman microscopy. *Plant Physiology*, 140(4), 1246–1254. DOI: 10.1104/pp.105.073395

[11] Schweingruber, F. H. (1996). *Tree rings and environment: Dendroecology*. Swiss Federal Institute for Forest, Snow and Landscape Research.

[12] Plomion, C., Leprovost, G., & Stokes, A. (2001). Wood formation in trees. *Plant Physiology*, 127(4), 1513–1523. DOI: 10.1104/pp.010816

[13] OGM (Orman Genel Müdürlüğü). (2023). Kastamonu Orman Bölge Müdürlüğü yıllık amenajman verileri. T.C. Tarım ve Orman Bakanlığı Yayınları.

[14] Zobel, B. J., & van Buijtenen, J. P. (1989). *Wood variation: Its causes and control*. Springer-Verlag.

[15] Zhang, S. Y., & Zhong, Y. (1992). Age and growth effects on wood density of hardwoods. *Wood Science and Technology*, 26(5), 393–400. DOI: 10.1007/BF00202250

[16] Körner, C., & Paulsen, J. (2004). A world-wide study of high altitude treeline temperatures. *Journal of Biogeography*, 31(5), 713–732. DOI: 10.1111/j.1365-2699.2003.01043.x

[17] Evans, J. D. (1996). *Straightforward statistics for the behavioral sciences*. Brooks/Cole Publishing.

[18] Panshin, A. J., & de Zeeuw, C. (1980). *Textbook of wood technology* (4th ed.). McGraw-Hill.

[19] Donaldson, L. A. (2001). Lignification and lignin topochemistry—An ultrastructural view. *Phytochemistry*, 57(6), 859–873. DOI: 10.1016/S0031-9422(01)00049-8

Research Article

JOURNAL OF CERAMICS AND COMPOSITES

e-ISSN: 3062-293X

A brief review on carbon nanotube-reinforced composites

Levent TURAN [a], Bekir AKGÖZ [b,*]

[a] Department of Civil Engineering, Faculty of Engineering, Akdeniz University, Antalya, 07070, Türkiye
[b] Department of Civil Engineering, Faculty of Engineering, Akdeniz University, Antalya, 07070, Türkiye

Highlights

- History of nanotechnology
- Various applications of nanotechnology
- Carbon nanotube
- Types of reinforced composites

Abstract

With the development of technology, scientists can now process atoms at the atomic scale. This enabled the development of nanotechnology. The development of nanotechnology has led to the production of some superior materials at micro and nano scales. Carbon nanotubes are an indispensable product for composite materials due to their high thermal properties, high electrical properties and high mechanical properties. Carbon nanotube-reinforced composites, which find their place in many areas such as engineering structures, the aerospace industry, medicine, and military applications, are a material that provides convenience for humanity. The developing world contributes to the development of humanity with its constant innovation and new discoveries every day. In this study, the properties of carbon nanotube reinforced composites, their areas of use, and their contributions to humans and the future were examined.

Information

Received:
04.02.2025
Received in revised:
07.03.2025
Accepted:
12.03.2025

Keywords: *Nanotechnology, carbon nanotube, reinforced composites*

1. Introduction

The term nano comes from Greek and means dwarf. Physically, 1 nanometer corresponds to 10^{-9} meters. Sizes between 1 and 100 nanometers are considered nanoscale [1,2]. All materials in our world are made up of atoms. The only differences between them are the types of atoms they are made of, their bonds, or the way they interact chemically. The properties of a material at the nanoscale differ from its properties at a larger scale. There are several reasons for this difference. But the most important one can be expressed as the surface area of materials at the nanoscale is much larger than the mass of the same material at larger scales [3]. The surface area to volume ratio a nanoparticle is given in Figure 1.

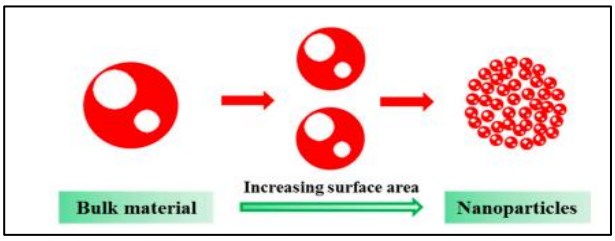

Figure 1. Nanoparticle surface area to volume ratio [4]

As materials become more chemically reactive at nanoscale, the electrical, magnetic, morphological, structural, thermal, optical and mechanical properties of the material are affected [5,6]. The properties of materials at nanoscale become difficult to explain with classical mechanical methods and quantum mechanics methods are used to determine these properties [7-9].

The synthesis of these nano-sized materials has enabled the emergence of extraordinary materials such as reinforced composites, advanced optical applications, high-tech devices, and superconductors [10,11]. Therefore, nanotechnology has an important place in human life.

2. History of Nanotechnology

The beginning of nanotechnology dates back to a speech given by American physicist Richard Feynman at a meeting of the association in 1959 [12]. In his speech, he mentioned that the atoms of matter could be intervened. The term nanotechnology was first defined by Norio Taniguchi at a conference in 1974 [13]. Kim Eric Drexler,

* Corresponding author: bekirakgoz@akdeniz.edu.tr (B., Akgöz), +90 242 310 6360

who guided his work with Richard Feynman's ideas, began to develop the concept of molecular nanotechnology and published his book The Coming Era of Nanotechnology in 1986. In his book, he aimed to use molecular structures at nanoscale to enable the synthesis of large molecules [14]. This and similar nano studies have increased every year.

Undoubtedly the most important advances in nanotechnology came with the invention of the scanning tunneling microscope in 1981 [15]. In 1989, IBM scientists used the scanning tunneling microscope to position atoms and form the letters IBM. Figure 2 shows the using a scanning tunneling microscope to form the letters IBM. This was a study that confirmed American physicist Richard Feynman.

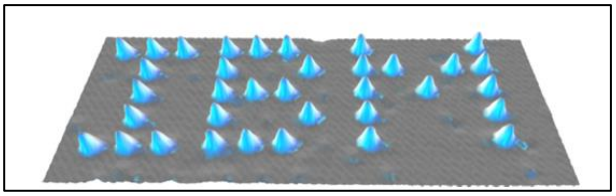

Figure 2. The letters "IBM" written in atoms using a scanning tunneling microscope [16]

With the studies we can see the properties of materials at the nanoscale. Of course, nanotechnology and nanoscience are complementary fields and there are aspects where these fields are superior to each other. According to some scientists, it is difficult to define these fields [17]. Science is the basis of technology and they are in constant interaction with each other.

2.1. Production of nanomaterials

The production of nanomaterials falls into two categories: top-down and bottom-up [18,19].

Top-down: materials are reduced to the nanoscale. It is the most common application of nanotechnology. It is widely used in the field of electronics. The disadvantage of this application is that the material is lost at some stages in the nanoscale [20].

Bottom-up: aims to achieve a whole with nanoscale materials. This application is called "true" nanotechnology and allows the material to be controlled. This application is also used in the production of carbon nanotubes [21].

2.2. Applications of nanotechnology

The remarkable properties at the nanoscale are giving rise to new applications every day. Scientists believe that the future will be shaped by the properties provided by nanomaterials. Nanotechnology covers almost many areas from the simplest to the most complex applications [22,23]. A few of these are:

2.2.1. Medicine

Nanotechnology has made a name for itself in the field of medicine. For example, the use of nano-silver in the treatment of wounds, the use of nanomaterials with high electronic and optical properties in the detection of cancer cells by acting as a fluorescent effect, and it contributes to human health in many ways [24-26].

While nanomaterials are used to deliver chemotherapy drugs to cancer cells, nanocapsules also contribute to the scientific world in destroying cancer cells [27-31]. Cancer diagnosis and treatment with nanotechnology is shown in Figure 3.

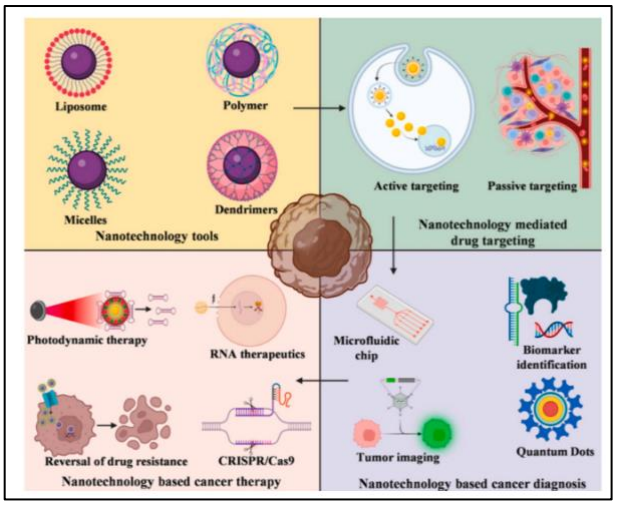

Figure 3. Cancer diagnosis and treatment with nanotechnology [32]

2.2.2. Aviation and space

Many parts of aircraft are manufactured with composites produced with the help of nanomaterials. The main purpose of this is the need for weight reduction. It is known that nanomaterials can show high mechanical properties at low weight. Corrosion and fatigue resistance properties are also used in the weight distribution [33-35].

The advantages of nanotechnology are also used in space research. Due to the high cost of materials sent to space, scientists are planning to make a space elevator with the help of nanomaterials [36,37].

2.2.3. Electronics

Nanomaterials have enabled extra thin and flexible designs in the field of electronics. In the future, small, light and modern technological products will be offered to the service of humanity thanks to nanomaterials [38,39]. The image created on the plastic film is shown in Figure 4.

2.2.4. Energy

Nowadays, energy storage devices such as batteries, fuel cells and cells are designed with nanotechnology. Various nanostructures such as carbon nanotubes and graphite nanofibers are used in the storage of hydrogen [41-43].

Nanotechnology has an important place in the storage of alternative energy. Thanks to it, environmental pollution will be reduced and more efficient energy use will be provided [44,45].

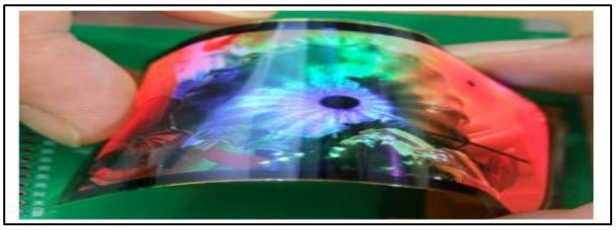

Figure 4. The image created on plastic film [40]

2.2.5. Textiles

The textile world is constantly evolving with new applications of developing technology. The durability of textile products, the texture of their fabrics, their sweat-proofing, flame-resistant and dirt-proofing features are at the forefront. Of course, these features are made possible by nanomaterials. Clothes that can change their properties according to the differences in our environment can be produced [46,47]. Applications of nanotechnology in textile are given in Figure 5.

Figure 5. Applications of Nanotechnology in textile industry [48]

2.2.6. Sports

In the field of sports, materials such as nanotextiles, nanoparticles, carbon nanotubes are used in the production of equipment that is more useful and provides maximum performance to the athlete. Of course, the adaptation of these nanoelements to textiles will allow the examination of the human body during sports and will eliminate unwanted situations such as possible injuries [49,50].

3. Carbon Nanotube

Carbon nanotubes are an indispensable part of nanotechnology. Carbon nanotubes, consisting of only carbon atoms with atomic number 6, were discovered by lijima and are widely used in nanotechnological applications. [51]. These nanotubes, consisting of carbon atoms, are a nano-sized tube-shaped material [52]. Carbon nanotube types are given in Figure 6.

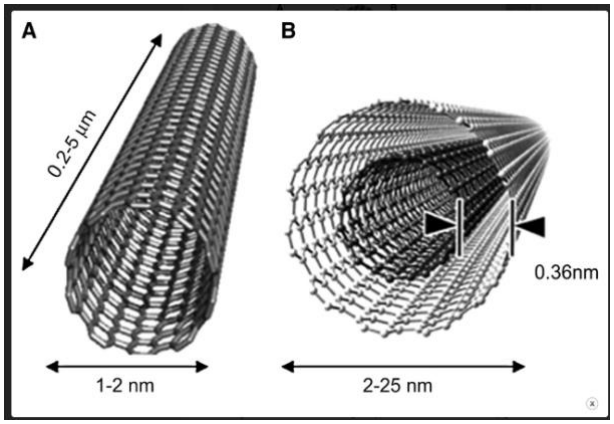

Figure 6. (A) Single-walled carbon nanotube (SWCNT) and (B) multi-walled carbon nanotube (MWCNT) [53]

Nano-sized carbons are used in high-strength composites, energy storage areas, semiconductor devices, sensors and many other areas [54-58]. Nanotubes have a higher elastic modulus than steel and since they have a higher tensile strength than steel, they are also used in structural elements and the automotive sector [59-61]. These high properties of carbon nanotubes make it an indispensable material for composite reinforcement [62, 63].

4. Reinforced Composites

Due to the high properties of carbon nanotubes, it has been used in the production of reinforced composite materials and has created a new research area [64]. Recently, many papers have been published in the literature about the mechanical analyses of carbon nanotube-reinforced composite beams [65-74]. Four different distribution patterns are seen in Figure 7 [65].

Composite materials are materials that consist of two or more materials with different physical or chemical properties and exhibit properties superior to those before they are combined [75]. The components of a composite are shown in Figure 8. They usually consist of additives placed in a matrix (polymer, metal or ceramic) [76]. When properly formed, the new material exhibits properties that exceed those of its constituent materials. These

properties include high strength, high toughness, corrosion resistance and fire resistance.

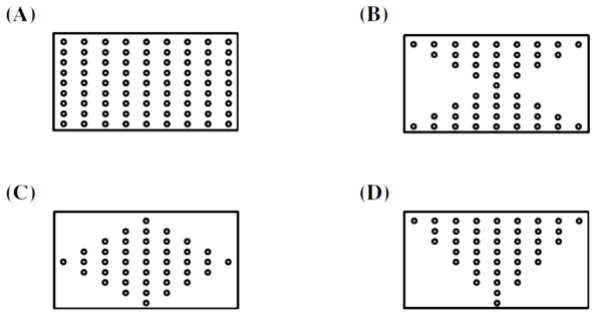

Figure 7. Various distribution patterns of carbon nanotubes: A) UD, B) FG-X, C) FG-O, and D) FG-V [65]

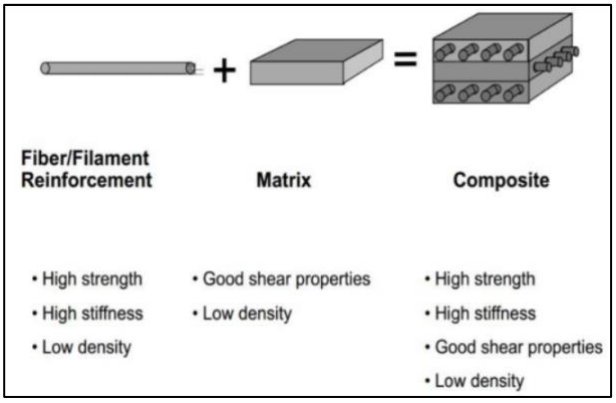

Figure 8. Components of composite [76]

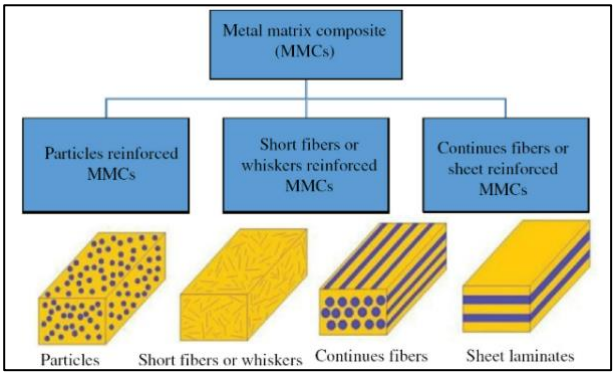

Figure 9. Types of metal matrix composites [81]

4.1. Metal matrix composites

Metal matrix composites consist of a metal or non-metal alloy matrix and reinforcement materials added to this matrix [77-79]. Types of metal matrix composites are given in Figure 9. Metal matrix composites, mostly used in the automobile and aviation industries, reduce the weight of the vehicles used and improve some mechanical properties [80]. Thus, high strength, high wear resistance, corrosion resistance and low fuel consumption are provided.

4.2. Ceramic matrix composites

Ceramic matrix composites consist of a ceramic matrix and reinforcement materials added to this matrix. The classification of ceramic matrix composites according to structure of matrix is given in Figure 10. They are widely used in hypersonic aircraft, thermal protection systems of spacecraft and turbine engines [82].

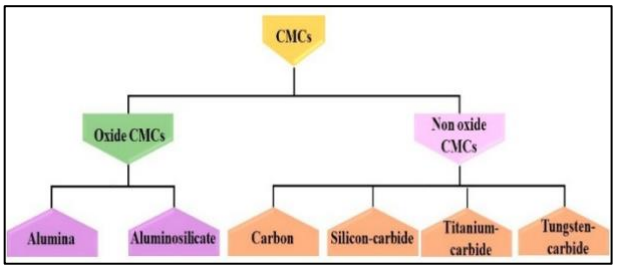

Figure 10. Classification of ceramic matrix composites according to the structure of the matrix [83]

4.3. Polymer matrix composites

Polymer matrix composites consist of a polymer matrix and reinforcement materials added to this matrix. Polymer matrix types are given in Figure 11. It has an important place because it shows higher physical, mechanical and thermal properties than other types [84]. Natural fibers have been used to develop these composites [85]. The right fiber and polymer selection is vital for the matrix [86,87].

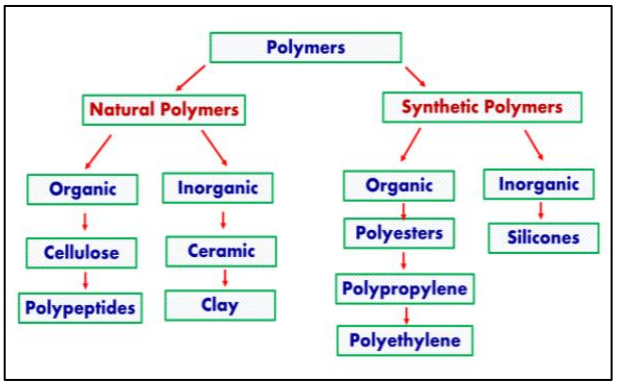

Figure 11. Types of polymers [88]

5. Conclusion

The existence of nanotechnology is an indispensable element for our present and future in terms of humanity. By adding nanomaterials to composite materials, they are provided with higher properties and more environmentally friendly. Nanotechnological products, which have a wide range of uses from sports to textiles, from medicine to space, will open the door to the next era of humanity. Every study in the field of nanotechnology is seen as a step towards achieving this goal.

Declaration of Interest Statement

The authors declare that they have no known competing financial interests or personal relationships that could have appeared to influence the work reported in this paper.

References

[1] Saleh, T.A. (2020). Nanomaterials: classification, properties, and environmental toxicities. *Environmental Technology & Innovation, 20*, 101067. DOI: 10.1016/j.eti.2020.101067

[2] Albanese, A., Tang, P.S., Chan, W.C. (2012). The effect of nanoparticle size, shape, and surface chemistry on biological systems. *Annual Review of Biomedical Engineering, 14*, 1–16. DOI: 10.1146/annurev-bioeng-071811-150124

[3] Loos, M. (2015). Carbon Nanotube Reinforced Composites. Elsevier.

[4] Sun, X., Zhang, Y., Chen, G., Gai, Z. (2017). Application of Nanoparticles in Enhanced Oil Recovery: A Critical Review of Recent Progress. *Energies, 10(3)*, 345. DOI: 10.3390/en10030345

[5] Muench, F. (2018). Metal Nanotube/Nanowire-Based Unsupported Network Electrocatalysts. *Catalysts, 8(12)*, 597. DOI: 10.3390/catal8120597

[6] Burhan, H., et al. (2023). Highly Efficient Carbon Hybrid Supported Catalysts Using Nano –Architecture As Anode Catalysts For Direct Methanol Fuel Cells. *International Journal of Hydrogen Energy, 48(17)*, 6657–6665. DOI: 10.1016/j.ijhydene.2021.12.141

[7] Gleiter, H. (1989). Nanocrystalline materials. *Progress in Materials Science, 33(4)*, 223-315. DOI: 10.1016/0079-6425(89)90001-7

[8] Watanabe, H. (1986). The Physics and Fabrikation of Microstructures and Microdevices (edited by Kelly M. J. and Weisbuch C.). Springer-Verlag, Berlin, p. 158.

[9] Inoshıta, T., Watanabe, H. (1987). Microclusters (edited by Sugano, S., Nishina, Y., Ohnishi, S.). Springer-Verlag, Tokyo, p. 281.

[10] An, Y., et al. (2021). Dealloying: An Effective Method for Scalable Fabrication of 0D, 1D, 2D, 3D Materials and Its Application in Energy Storage. *Nano Today, 37*, 101094. DOI: 10.1016/j.nantod.2021.101094

[11] Arenal, R., Lopez- Bezanilla, A. (2015). Boron Nitride Materials: An Overview From 0D to 3D Structures. *Wires Computational Molecular Science, 5(4)*, 299–309. DOI: 10.1002/wcms.1219

[12] Minoli, D. (2005). Nanotechnology applications to telecommunications and networking. 1st ed., John Wiley and Sons.

[13] Hornyak, G.L., Tibbals, H.F., Dutta, J., Moore, J.J. (2009). Introduction to nanoscience and nanotechnology. Taylor and Francis, LLC.

[14] Drexler, K. E. (1986). Engines of Creation: The Coming Era of Nanotechnology.

[15] Surface Sciences., C. Bai Scanning Tunneling Microscopy and Its Applications, Second Revised Edition, Shanghai Scientific & Technical Publishers.

[16] Eiger, D.M., Schweizer E. K. (1990). Positioning single atoms with a scanning tunneling microscope. *Nature, 344*, 524-526. DOI: 10.1038/344524a0

[17] Collins, P.G., Avouris, P. (2000). Nanotubes for electronics. *Scientific American, 62(283)*, 69. DOI: 10.1038/scientificamerican1200-62

[18] Miller, J.C., Serrato, R.M., Represas-Cardenas, J.M., Kundahl, G. (2004). The handbook of nanotechnology business, policy, and intellectual property law. 1st ed., Wiley.

[19] Madhumitha, G., Roopan, S.M. (2013). Devastated crops: Multifunctional efficacy for the production of nanoparticles. *Journal of Nanomaterials, 1*, 951858. DOI: 10.1155/2013/951858

[20] Ijaz, I., Gilani, E., Nazir, A., Bukhari, A. (2020). Detail review on chemical, physical and green synthesis, classification, characterizations and applications of nanoparticles. *Green Chemistry Letters and Reviews, 13(3)*, 59–81. DOI: 10.1080/17518253.2020.1802517

[21] Rothemund, P.W.K. (2006). Folding dna to create nanoscale shapes and patterns. *Nature, 440*, 297-302. DOI: 10.1038/nature04586

[22] Hulla, J.E., Sahu, S.C., Hayes, A.W. (2015). Nanotechnology: History and future. *Human & Experimental Toxicology, 34(12)*, 1318-1321. DOI: 10.1177/0960327115603588

[23] Pagliaro, M. (2011). Nano-Age: How Nanotechnology Changes Our Future. John Wiley & Sons.

[24] Alavi, M., Varma, R.S. (2021). Antibacterial and wound healing activities of silver nanoparticles embedded in cellulose compared to other polysaccharides and protein polymers. *Cellulose, 28*, 8295–8311. DOI: 10.1007/s10570-021-04067-3

[25] Singh, M., Thakur, V., Kumar, V., Raj, M., Gupta, S., Devi, N., Upadhyay, S.K., Macho, M., Banerjee, A., Ewe, D., Saurav, K. (2022). Silver nanoparticles and its mechanistic insight for chronic wound healing: review on recent progress. *Molecules, 27(17)*, 5587. DOI: 10.3390/molecules27175587

[26] Haidari, H., Garg, S., Vasilev, K., Kopecki, Z., Cowin, A.J. (2020). Silver-based wound dressings: current issues and future developments for treating bacterial infections. *Wound Practice and Research, 28(4)*, 173-180. DOI: 10.33235/wpr.28.4.173-180

[27] Roldo, M., Fatouros, D.G. (2013). Biomedical applications of carbon nanotubes. *Annual Reports Section C-Physical Chemistry, 109*, 10–35. DOI: 10.1039/c3pc90010j

[28] Kesharwani, P., Ghanghoria R., Jain N. K. (2012). Carbon nanotube exploration in cancer cell lines. *Drug Discovery Today, 17*, 1023–1030. DOI: 10.1016/j.drudis.2012.05.003

[29] Hosseini, S.M., Mohammadnejad, J., Salamat, S., Beiram Zadeh, Z., Tanhaei, M., Ramakrishna, S. (2023). Theranostic polymeric nanoparticles as a new approach in cancer therapy and diagnosis: a review. *Materials Today Chemistry, 29*, 101400. DOI: 10.1016/J.MTCHEM.2023.101400

[30] Yap, K.M., Sekar, M., Fuloria, S., Wu, Y.S., Gan, S.H., Mat Rani, N.N.I., Subramaniyan, V., Kokare, C., Lum, P.T., Begum, M.Y., Mani, S., Meenakshi, D.U., Sathasivam, K.V., Fuloria, N.K. (2021). Drug delivery of natural products through nanocarriers for effective breast cancer therapy: a comprehensive review of literature. *International Journal of Nanomedicine, 16*, 7891–7941. DOI: 10.2147/IJN.S328135

[31] Das, S., Dey, M.K., Devireddy, R., Gartia, M.R. (2024). Biomarkers in cancer detection, diagnosis, and prognosis. *Sensors, 24(1)*, 37. DOI: 10.3390/S24010037

[32] Tiwari, H., et al. (2023). Recent advances in nanomaterials-based targeted drug delivery for preclinical cancer

diagnosis and therapeutics. *Bioengineering, 10*, 760. DOI: 10.3390/BIOENGINEERING10070760

[33] Jingxuan, H. (2024). Nanomaterials in aerospace: Revolutionizing flight and exploration through nanoscale advancements. *Applied and Computational Engineering, 60*, 1-5. DOI: 10.54254/2755-2721/60/20240821

[34] Tiwary, A., Kumar, R., Chohan, J.S. (2022). A review on characteristics of composite and advanced materials used for aerospace applications. Materials Today: Proceedings. DOI: 10.1016/j.matpr.2021.06.276

[35] Norkhairunnisa, M., Chai, Hua, T., Sapuan, S.M., Ilyas, R.A. (2022). Evolution of aerospace composite materials. In Advanced composites in aerospace engineering applications, (pp. 367- 385), Cham: Springer International Publishing. DOI: 10.1007/978-3-030-88192-4_18

[36] Clarke, A.C. (1979). The Space Elevator: 'Thought Experiment', or Key to the Universe, Advanced Earth Oriented Applied Science Technology 1:39.

[37] Edwards, B.C., Westling, E.A. (2002). The Space Elevator, San Jose: Spa geo.

[38] Nathan, A., Ahnood, A., Cole, M. T., Lee, S., Suzuki, Y., Hiralal, P., Bonaccorso, F., Hasan, T., Garcia Gancedo, L., Dyadyusha, A. (2012). Flexible Electronics: The Next Ubiquitous Platform. *Proceedings of the IEEE, 100(13)*, 1486-1517.

[39] Imazu, N., Fujigaya, T., Nakashima, N. (2014). Fabrication of flexible transparent conductive films from long double-walled carbon nanotubes. *Science & Technology of Advanced Materials*, 15 (2), 025005. DOI: 10.1088/1468-6996/15/2/025005

[40] An, S., Lee, J., Kim, Y., Kim, T., Jin, D., Min, H., Chung, H., Kim, S.S. (2010). 47.2: 2.8-Inch WQVGA flexible AMOLED using high performance low temperature polysilicon TFT on plastic substrates. In 48th Annual SID Symposium, Seminar, and Exhibition 2010, Display Week 2010; Blackwell Publishing Ltd.: Oxford, UK, Volume 41, pp. 706–709. DOI: 10.1889/1.3500566

[41] Züttel, A., Sudan, P., Mauron, Ph., Kiyobayashi, T., Emmenegger, Ch., Schlapbach, L. (2002). Hydrogen storage in carbon nanostructures. *International Journal of Hydrogen Energy, 27*, 203–212. DOI: 10.1016/S0360-3199(01)00108-2

[42] Schimmel, H.G., Kearley, G.J., Nijkamp, M.G., Visserl, C.T., Jong de, K.P., Mulder, F.M. (2003). Hydrogen adsorption in carbon nanostructures compared. *Materials Science Engineering B, 108*, 124–129. DOI: 10.1016/j.mseb.2003.10.091

[43] Dresselhaus, M.S., Williams, K.A., Eklund, P.C. (1999). Hydrogen adsorption in carbon materials. *MRS Bull, 24*, 45–50. DOI: 10.1557/S0883769400053458

[44] Aithal, P.S., Shubhrajyotsna, A. (2018). Nanotechnology based Innovations and Human Life Comfortability –Are we Marching towards Immortality. *International Journal of Applied Engineering and Management Letters, 2(2)*, 71-86. DOI: 10.5281/zenodo.1451498

[45] Aithal, P. S., Shubhrajyotsna, A. (2018). Study of various General-Purpose Technologies and their contribution towards developing Sustainable Society. *International Journal of Management, Technology, and Social Sciences, 3(2)*, 16-33. DOI: 10.5281/zenodo.1409476

[46] Pereira, C., Pereira, A.M., Freire, C., Pinto, T.V., Costa, R.S., Teixeira, J.S. (2020). Nanoengineered textiles: from advanced functional nanomaterials to groundbreaking high-performance clothing. In: Handbook of Functionalized Nanomaterials for Industrial Applications, Mustansar Hussain, C., Ed. Elsevier, p. 611–714. DOI: 10.1016/b978-0-12-816787-8.00021-1

[47] Chen, J., Zhan, Y., Wang Y., Han, D., Tao, B., Luo, Z., et al. (2018). Chitosan/silk fibroin modified nanofibrous patches with mesenchymal stem cells prevent heart remodeling post-myocardial infarction in rats. *Acta Biomaterialia, 80*, 154–168. DOI: 10.1016/j.actbio.2018.09.013

[48] Yetişen, A.K., Qu, H., Manbachi, A., Butt, H., Dokmeci, M.R., Hinestroza, J.P., Skorobogatiy, M., Khademhosseini, A., Yun, S.H. (2016). Nanotechnology in Textiles. *ACS Nano, 10(3)*, 3042-3068. DOI: 10.1021/acsnano.5b08176

[49] Saad, E.R. (2021). Applications of Nanotechnology in Production of Smart Sportswear. *Journal of Architecture, Arts and Humanities, 2(1)*, 681-694. DOI: 10.21608/mjaf.2020.46501.1954

[50] Harifi, T., Montazer, M. (2017). Application of Nanotechnology in Sports Clothing and Flooring for Enhanced Sports Activities, Performance, Efficiency and Comfort: A Review. *Journal of Industrial Textiles, 46(5)*, 1147–1169. DOI: 10.1177/1528083715601512

[51] Iijima, S. (1991). Helical microtubules of graphitic carbon. *Nature, 354*, 56-58. DOI: 10.1038/354056a0

[52] Kaushik, B.K., Majumder, M.K. (2015). Carbon nanotube based VLSI interconnects. Analysis and design, New Delhi: Springer India, pp. 1-14. DOI: 10.1007/978-81-322-2047-3_1

[53] Singh, I., Rehni, A.K., Pradeep, K., Manoj, K., Hassan Y.A. (2009). Carbon Nanotubes: Synthesis, Properties and Pharmaceutical Applications. *Fullerenes Nanotubes and Carbon Nanostructures*, 361-377. DOI: 10.1080/15363830903008018

[54] Lee, J., Kim, T., Jung, Y., Jung, K., Park, J., Lee, D.M., Kim, S.M. (2016). High-strength carbon nanotube/carbon composite fibers via chemical vapor infiltration, *Nanoscale, 8(45)*, 18972-18979. DOI: 10.1039/C6NR06479E

[55] Arunachalam, S., Gupta, A.A., Izquierdo, R., Nabki, F. (2018). Suspended carbon nanotubes for humidity sensing. *Sensors, 18(5)*, 1655. DOI: 10.3390/s18051655

[56] Xu, J.L., Dai, R.X., Xin, Y., Sun, Y.L., Li, X., Yu, Y.X., Ren, T.L. (2017). Efficient and reversible electron doping of semiconductor-enriched single-walled carbon nanotubes by using decamethylcobaltocene. *Scientific Reports, 7(1)*:, 1-10. DOI: 10.1038/s41598-017-05967-w

[57] Kumar, S., Nehra, M., Kedia, D., Dilbaghi, N., Tankeshwar, K., Kim, KH. (2018). Carbon nanotubes: A potential material for energy conversion and storage. *Progress in Energy and Combustion Science, 64*, 219-253. DOI: 10.1016/j.pecs.2017.10.005

[58] Yu, MF., Files, BS., Arepalli, S., Ruoff, RS. (2000). Tensile loading of ropes of single wall carbon nanotubes and their mechanical properties. *Physical Review Letters, 84(24)*, 5552. DOI: 10.1103/PhysRevLett.84.5552

[59] Tostenson, E.T., Ren, Z.F., Chou, T.W. (2001). Advances in the science and technology of carbon nanotubes and their composites: a review. *Composite Science and Technology, 61*. DOI: 10.1016/S0266-3538(01)00094-X

[60] Krishnan, A., Shandilya, S., Gupta, P., Balu, H. (2020). A Review on Applications of Carbon Nanotubes in Automobiles. *International Journal of Mechanical Engineering and Technology, 11*, 204-210. DOI: 10.34218/IJMET.11.1.2020.018

[61] Taub, A., Luo, A. (2015). Advanced lightweight materials and manufacturing processes for automotive applications. *MRS Bulletin, 40*, 1045-1054. DOI: 10.1557/mrs.2015.268

[62] Danafar, F., Kalantari, M. (2018). A review of natural rubber nanocomposites based on carbon nanotubes. *Journal of Rubber Research, 21*, 293–310. DOI: 10.1007/bf03449176

[63] Saifuddin, N., Raziah, AZ., Junizah, AR. (2013). Carbon nanotubes: a review on structure and their interaction with proteins. *Journal of Chemistry*, 676815. DOI: 10.1155/2013/676815

[64] Amal, M. K. E., Mahmoud, M. F. (2007). Carbon nanotube reinforced composites: Potential and current challenges. *Materials & Design, 28*, 2394-2401. DOI: 10.1016/j.matdes.2006.09.022

[65] Civalek, Ö., Dastjerdi, S., Akbaş, Ş. D., Akgöz, B. (2021). Vibration analysis of carbon nanotube-reinforced composite microbeams. *Mathematical Methods in the Applied Sciences*, 1–17. DOI: 10.1002/mma.7069

[66] Ke, L.L., Yang, J., Kitipornchai, S. (2010). Nonlinear free vibration of functionally graded carbon nanotube-reinforced composite beams. *Composite Structures, 92(3)*, 676-683. DOI: 10.1016/j.compstruct.2009.09.024

[67] Yas, M.H., Heshmati, M. (2012). Dynamic analysis of functionally graded nanocomposite beams reinforced by randomly oriented carbon nanotube under the action of moving load. *Applied Mathematical Modelling, 36(4)*, 1371-1394. DOI: 10.1016/j.apm.2011.08.037

[68] Yas, M.H., Samadi, N. (2012). Free vibrations and buckling analysis of carbon nanotube-reinforced composite Timoshenko beams on elastic foundation. *International Journal of Pressure Vessels and Piping, 98*, 119-128. DOI: 10.1016/j.ijpvp.2012.07.012

[69] Uzun, B., Yaylı, M.Ö. (2024). Free Vibration of a Carbon Nanotube-Reinforced Nanowire/Nanobeam with Movable Ends. *Journal of Vibration Engineering and Technology, 12*, 6847–6863. DOI: 10.1007/s42417-024-01287-2

[70] Wattanasakulpong, N., Ungbhakorn, V. (2013). Analytical solutions for bending, buckling and vibration responses of carbon nanotube-reinforced composite beams resting on elastic foundation. *Computational Materials Science, 71*, 201-208. DOI: 10.1016/j.commatsci.2013.01.028

[71] Ozdemir, O., Esen, I., Ural, H. (2023). Vibration response of rotating carbon nanotube reinforced composites in thermal environment. *Steel and Composite Structures, 47*, 1-17. DOI: 10.12989/scs.2023.47.1.001

[72] Civalek, Ö., Akbaş, Ş. D., Akgöz, B., Dastjerdi, S. (2021). Forced Vibration Analysis of Composite Beams Reinforced by Carbon Nanotubes. *Nanomaterials, 11(3)*, 571. DOI: 10.3390/nano11030571

[73] Akbas, S.D., Numanoglu, H.M., Akgöz, B., Civalek, Ö. (2022). Application of Newmark Average Acceleration and Ritz Methods on Dynamical Analysis of Composite Beams under a Moving Load. *Journal of Applied and Computational Mechanics, 8(2)*, 764-773. DOI: 10.22055/jacm.2022.39345.3393

[74] Avcar, M., Hadji, L., Civalek, Ö. (2023). The influence of non-linear carbon nanotube reinforcement on the natural frequencies of composite beams, *Advances in Nano Research, 14(5)*, 421-433. DOI: 10.12989/anr.2023.14.5.421

[75] Amjad, A., Rahman, A.A.A., Awais, H., Zainol Abidin, M.S., Khan J. (2022). A review investigating the influence of nanofiller addition on the mechanical, thermal and water absorption properties of cellulosic fibre reinforced polymer composite. *Journal of Industrial Textiles, 51(1)*, 65S-100S. DOI: 10.1177/15280837211057580

[76] Kumar, Y.K., Lohchab, D.S. (2016). Influence of aviation fuel on mechanical properties of glass fiber-reinforced plastic composite. *International Advanced Research Journal in Science, Engineering and Technology, 3(4)*, 58-65. DOI: 10.17148/IARJSET.2016.3413

[77] Chawla, N., Chawla, K.K. (2006). Metal Matrix Composites. Springer, NY, USA. DOI: 10.1007/978-1-4614-9548-2

[78] Safri, S., Sultan, M., Jawaid, M., Jayakrishna, K. (2018). Impact behaviour of hybrid composites for structural applications: a review. *Composites Part B-Engineering, 133*, 112–121. DOI: 10.1016/j.compositesb.2017.09.008

[79] Ekka, KK., Chauhan, SR. Varun. (2014). Dry sliding wear characteristics of SiC and Al2O3 nanoparticulate aluminium matrix composite using Taguchi technique. *Arabian Journal for Science and Engineering, 40*, 571–581. DOI: 10.1007/s13369-014-1528-2

[80] Kok, M. (2005). Production and mechanical properties of Al2O3 particle-reinforced 2024 aluminium alloy composites. *Journal of Materials Processing Technology, 161*, 381–387. DOI: 10.1016/j.jmatprotec.2004.07.068

[81] Mistry, JM., Gohil, PP. (2018). Research review of diversified reinforcement on aluminium metal matrix composites: fabrication processes and mechanical characterization. *Science and Engineering of Composite Materials, 25(4)*, 633-647. DOI: 10.1515/secm-2016-0278

[82] Ruggles-Wrenn, M.B., Boucher N, Przybyla C. (2018). Fatigue of three advanced SiC/SiC ceramic matrix composites at 1200°C in air and in steam. *International Journal of Applied Ceramic Technology, 15*, 3-15. DOI: 10.1111/ijac.12773

[83] Shrivastava, S., Rajak, D. K., Joshi, T., Singh D. K., Mondal, D. P. (2024). Ceramic Matrix Composites: Classifications, Manufacturing Properties and Applications. *Ceramics, 7(2)*, 652-679. DOI: 10.3390/ceramics7020043

[84] Nagaraj, N., Balasubramaniam, S., Venkataraman, V., Manickam, R., Nagarajan, R., Sikiru Oluwarotimi, I. (2020). Effect of cellulosic filler loading on mechanical and thermal properties of date palm seed/vinyl ester composites. *International Journal of Biological Macromolecules, 147*, 53–66. DOI: 10.1016/j.ijbiomac.2019.11.247

[85] Shiva Kumar, K., Chennakesava Reddy, A. (2020). Investigation on mechanical properties and wear performance of Nylon-6/Boron Nitride polymer composites by using Taguchi Technique. *Results in Materials, 5*, 100070. DOI: 10.1016/j.rinma.2020.100070

[86] Al-Oqla, F.M., Sapuan, S.M. (2014). Natural fiber reinforced polymer composites in industrial applications: Feasibility of date palm fibers for sustainable automotive industry. *Journal of Cleaner Production, 66*, 347–354. DOI: 10.1016/j.jclepro.2013.10.050

[87] Dalmis, R., Köktaş, S., Seki, Y., Kılınç, A.Ç. (2020). Characterization of a new natural cellulosebased fiber from *Hierochloe Odarata*. *Cellulose, 27*, 127–139. DOI: 10.1007/s10570-019-02779-1

[88] Ravichandran, M., Balasubramanian, M., Chairman, CA., Pritima, D., Dhinakaran, V., Stalin, B. (2020). Recent developments in polymer matrix composites–a review. *IOP Conference Series: Materials Science and Engineering, 988(1)*, 012096. DOI: 10.1088/1757-899X/988/1/012096